Materials Science & Engineering C 127 (2021) 112199

Contents lists available at ScienceDirect

Materials Science & Engineering C

journal homepage: www.elsevier.com/locate/msec

Review

Multifunctional theranostic nanoparticles for biomedical cancer treatments - A comprehensive review

Ganeshlenin Kandasamy [a], Dipak Maity [b,*]

[a] Department of Biomedical Engineering, Vel Tech Rangarajan Dr. Sagunthala R&D Institute of Science and Technology, Chennai, India
[b] Department of Chemical Engineering, University of Petroleum and Energy Studies, Dehradun, India

ARTICLE INFO

Keywords:
Theranostic nanoparticles
Metal and magnetic nanoparticles
Hyperthermia
Near-infrared imaging
Photothermal therapy
Cancer treatment

ABSTRACT

Modern-day search for the novel agents (their preparation and consequent implementation) to effectively treat the cancer is mainly fuelled by the historical failure of the conventional treatment modalities. Apart from that, the complexities such as higher rate of cell mutations, variable tumor microenvironment, patient-specific disparities, and the evolving nature of cancers have made this search much stronger in the latest times. As a result of this, in about two decades, the theranostic nanoparticles (TNPs) – i.e., nanoparticles that integrate therapeutic and diagnostic characteristics – have been developed. The examples for TNPs include mesoporous silica nanoparticles, luminescence nanoparticles, carbon-based nanomaterials, metal nanoparticles, and magnetic nanoparticles. These TNPs have emerged as single and powerful cancer-treating multifunctional nanoplatforms, as they widely provide the necessary functionalities to overcome the previous/conventional limitations including lack of the site-specific delivery of anti-cancer drugs, and real-time continuous monitoring of the target cancer sites while performing therapeutic actions. This has been mainly possible due to the association of the as-developed TNPs with the already-available unique diagnostic (e.g., luminescence, photoacoustic, and magnetic resonance imaging) and therapeutic (e.g., photothermal, photodynamic, hyperthermia therapy) modalities in the biomedical field. In this review, we have discussed in detail about the recent developments on the aforementioned important TNPs without/with targeting ability (i.e., attaching them with ligands or tumor-specific antibodies) and also the strategies that are implemented to increase their tumor accumulation and to enhance their theranostic efficacies for effective biomedical cancer treatments.

1. Introduction

Cancer threatens human life and causes countless deaths globally [1]. Cancer is resulted due to a plethora of mutations in the genome of an individual which cause uncontrolled growth of cells. Approximately, 9.6 million people have died in 2018 due to cancer with 18.1 million new cases occur every year. Over the past two decades, several cancer studies have been performed with the aim to seek solutions for effective cancer treatment. Death by cancer mainly occurs due to late diagnostics and non-specific therapeutics [2]. There are different diagnostic methods for detecting various types of cancers–for instance, mammography for breast cancer, and the presence of specific antigens for prostate cancer [3,4]. Technological advancements in the fields of biomedical imaging instruments such as magnetic resonance imaging (MRI) and computed tomography (CT) have recently provided valuable insights about the different stages of cancer and its progression [5]. Despite all these advancements, more research is required to improve cancer diagnostics.

Another aspect of mortality due to cancer is mainly the therapeutic failure. Chemotherapy (CMT), radiation therapy (RDT), immunotherapy (IMT), and surgery are some of the basic treatment options for killing or hindering the growth of different types of cancer cells. However, there are several challenges or limitations associated with these conventional cancer treatment strategies such as low biodistribution of chemotherapeutic drugs (CTDs) which produce toxic effects to the healthy cells besides attacking the fast-growing cancer cells, extensive harmful radiations to normal tissues, and/or non-specific therapies [6]. Nevertheless, the differences in the tumor microenvironments in each cancer patient (as compared to the normal tissue environment) and the higher rate of accumulated new mutations are triggering cancer treatment failures additionally. Moreover, there are two distinct cell types within the tumor tissues – i.e., cancer stem cells and associated proliferating cells (which constitute a large mass of cells). Among these two, cancer stem

* Corresponding author.
E-mail address: dipakmaity@gmail.com (D. Maity).

https://doi.org/10.1016/j.msec.2021.112199
Received 9 March 2021; Received in revised form 12 May 2021; Accepted 18 May 2021
Available online 24 May 2021

cells can genetically reprogram themselves for (i) cell migration and (ii) developing multidrug resistance (MDR) against the cytotoxic drugs due to the increased multidrug resistance (MDR) associated protein pumps, known as p-glycoprotein (P-gp), which lead to escape the effects of chemotherapeutics and thus increase the proliferation of cancer tissues during or shortly after the therapy [7,8]. Besides, vasculature around the tumor environment is very dense to supply excessive nutrients (as compared to normal tissues), which results in the enormous growth of cancer cells [9].

To encounter these problems, in recent times, biocompatible theranostic nanoparticles (TNPs) are synthesized and applied in early detection, constant monitoring, and also the safe treatment of cancers, by integrating dual characteristics/functions – i.e., diagnostics and therapeutics. Moreover, in the ongoing quest to improve the theranostic efficacy, TNPs are prepared as functionalized nanoparticles by performing chemical modifications and/or bio-conjugations to evolve as new generation drug-delivery systems (DDS) for tumor-site-specific-targeting and selective & sustained release to increase tumor accumulation (by averting enhanced permeability and retention (EPR) effects by passing through biological barriers (e.g., blood-brain-barrier)), while eliminating or reducing all the possible side effects [10–12]. Apart from that, the TNPs have the capability to combine multiple imaging/therapeutic functionalities in a single nanoplatform (NPF) by attaching/associating themselves with distinct theranostic molecules/agents for use in imaging (CT-/MRI-/luminescence-/near-infrared-(NIR)) guided CMT, magnetic-hyperthermia-therapy (MHT), photodynamic therapy (PDT), photothermal therapy (PTT), etc.

Though many review articles have already discussed about the above-mentioned aspects of the TNPs, they are majorly focused on their functionalities in an individual manner. In addition, there is a severe lack of comprehensive studies about the lately made TNPs and their role in cancer treatments. Therefore, in this review, we have mainly discussed the recent developments in distinct TNPs that include (i) mesoporous silica nanoparticles, (ii) fluorescence/luminescence nanoparticles, (iii) carbon-based nanomaterials, (iv) metal nanoparticles, and (v) magnetic nanoparticles, and their multi-functionality characteristics (such as DDS, site-specific targeting (i.e., functionalized), and image-guided therapeutics) potential in a comprehensive manner for the treatment of different types of cancers.

2. Theranostic nanoparticles (TNPs)

TNPs have emerged as highly attractive and very promising candidates in cancer treatments as they possess innate therapeutic and/or diagnostic functions, along with drug-delivering capability. Herein, the recent developments on different multifunctional TNPs (MNTNPs) and

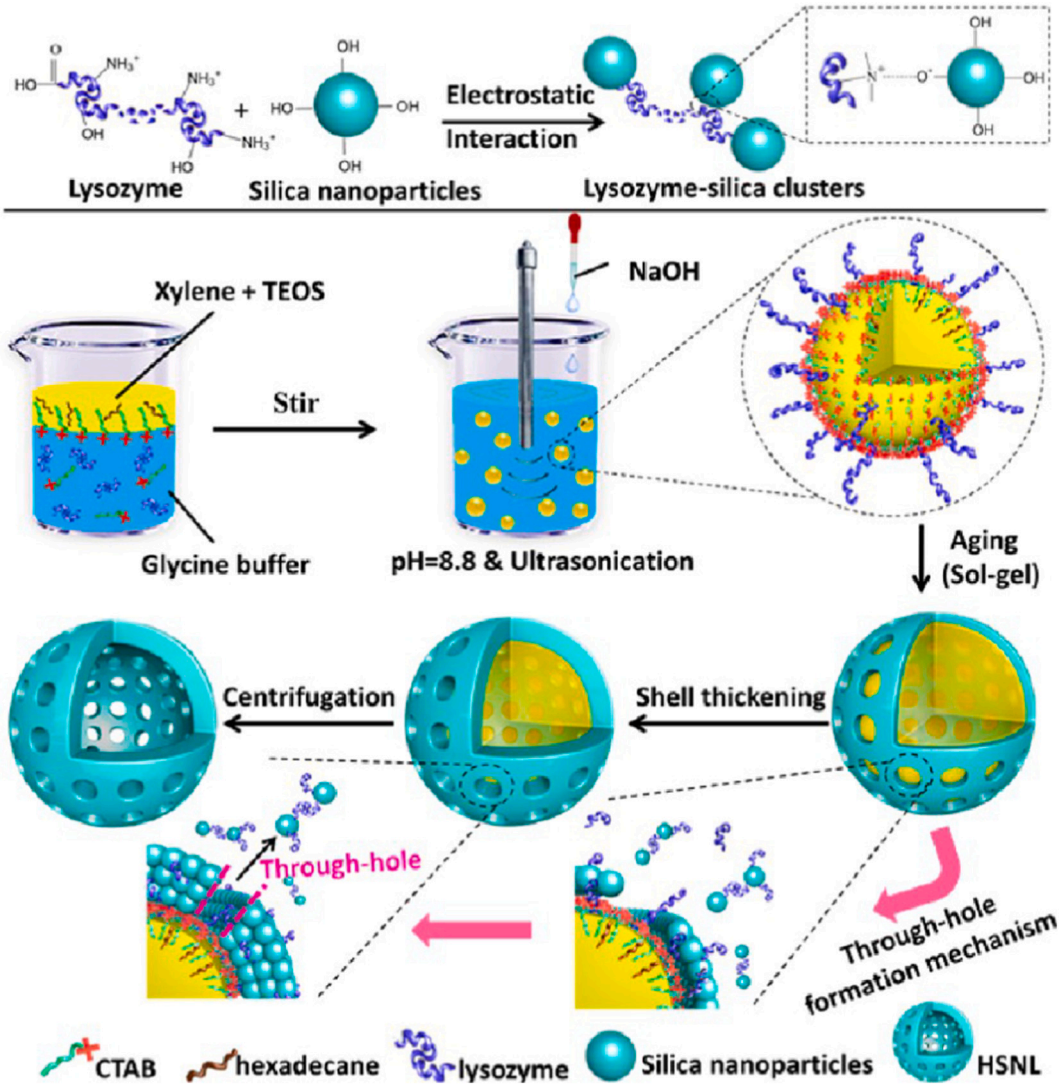

Fig. 1. Schematic illustration of the synthesis of HSNLs.
Adapted from Ref. [19].

their distinct biomedical cancer applications are discussed in detail.

2.1. Mesoporous silica nanoparticles

Mesoporous silica nanoparticles (MSNs) are utilized as potential DDS with high drug-carrying capability over the last few years. This is ascribed to their unique morphology, mono-distribution, tuneable particle sizes (50–300 nm) with uniform pore-size (2–6 nm), and pore-volume (to graft large amount of functional groups), excellent biocompatibility, thermal stability, exceptional physicochemical properties (for instance, colloidal stability/water dispersibility), versatile surface-chemistry, high surface-area and high loading capacity (ability to load different cargo molecules/agents) [13–15].

MSNs are usually prepared by sol-gel/Stöber process (refer Fig. 1) - i.e. hydrolysis of alkoxide precursor tetraethyl orthosilicate (TEOS) in the presence of surfactants such as cetyltrimethylammonium bromide (CTAB) [16–21]. Then, the surface of MSNs would be (i) modified with stabilizing coatings (e.g. polyethylene glycol (PEG)-ylation) to increase blood circulation half-life by evading reticuloendothelial system (RES) uptake, and/or (ii) functionalized with site-specific ligands (e.g. folate, mannose, transferrin, and peptides) or stimuli-responsive molecules (e.g. pH/enzyme-transformation/redox-reactions/temperature/light/magnetic-field) to produce smart/stealth, targeted and responsive DDS for effectively delivering the loaded cancer drugs at the interested sites [22–24]. For example, polyglutamic acid (PGA)-capped and rhodamine/doxorubicin (DOX – a CTD) loaded MSNs are developed as enzyme-controlled DDS with high water solubility, physicochemical stability, and improved biocompatibility with enhanced bioavailability [25]. These PGA-capped MSNs have shown selective drug release (20–90%) in the presence of pronase – ascribed to the hydrolysis of the peptide bonds in the polymer (i.e., PGA), and resulted in the effective killing (~90%) of SK-BR-3 based breast-cancer cells. Likewise, Cheng et al. have made enzyme-responsive MSNs based DDS by functionalizing them with α-cyclodextrin (α-CD) and peptide (azido-GFLGR7RGDS) [26]. The obtained DDS have exhibited high drug (DOX) loading (~80%) capacity, selective tumor targeting, improved cell uptake, and also cathepsin B-responsive drug release, which have consequently increased the growth inhibition rate in HeLa cells ($\alpha v\beta 3$ + ve). In another recent study, poly(2-(diethylamino)-ethyl methacrylate) (PDEAEMA)-conjugated and DOX-loaded MSNs are developed as pH−/reduction-/UV light-based triple stimuli-responsive DDS [27]. These MSNs have exhibited high drug loading capacity, boosted release, and effective internalization inside HeLa cancer cells while displaying a better control over the drug delivery via triple stimuli-responsiveness. Likewise, Poostforooshan et al. have reported the synthesis of pH-sensitive MSNs with large hollow interior cavity with tuneable porosity of permeable mesoporous shell and layer-by-layer surface-functionalized with two biocompatible polymers such as alginate and poly(allylamine hydrochloride) [28]. The as-formed MSNs have exhibited high drug loading efficiency (46% for the anticancer drug N6L), efficient pH-responsive drug release (at lower pH of tumors), and more than 60% of growth inhibition of pancreatic cancer cells.

Moreover, MSNs can be successfully designed as MNTNPs by associating with different nano-molecules/nanoparticles (such as super-paramagnetic iron oxide nanoparticles (SPIONs), gold, CuS, gelatin, and so on) and targeting agents along with the CTDs to achieve improved multimodal & synergistic theranostic efficacies while realizing better tumor-targeting, controlled/triggered drug delivery, reduced hostile effects of anticancer drugs, etc. [29–32]. For instance, Dai et al. have formed dendrimers-like MSNs with hierarchical pores (HPSNs) as pH-responsive MNTNPs for use in in vivo targeted cancer imaging and therapy [33]. Herein, HSPNs are functionalized with the following: Salphdc (*N*,*N*-phenylene bis(salicylideneimine)-dicarboxylic-acid – for pH-responsiveness) and indium ions (for fluorescence), DOX (model anti-cancer drug) and folic acid (FA – for targeting). Functionalization of MSNs has resulted in effective targeting, better-triggered drug release, good fluorescence-imaging-guided-treatment, and improved tumor growth inhibition. Similarly, Singh et al. have developed DOX-loaded fluorescent MSNs based MNTNPs with hollow nano-ellipsoid structure [34]. The as-prepared MSNs have displayed high drug loading capacity and sustained release, significant cell uptake, good biocompatibility, and enhanced fluorescence signals for cancer cell imaging. Likewise, Nakamura et al. have developed MSNs based MNTNPs by (i) loading DOX and ^{19}F MRI contrast agents inside their pores, (ii) labelling their surface with fluorescent dyes, and finally (iii) surface-conjugating them with FA targeting ligands [35]. These MNTNPs have enabled better-targeted drug delivery and also controlled drug release inside the cancer cells with bi-modal imaging capabilities (via NIR fluorescence imaging and ^{19}F MRI), thus improving the overall cancer treatments via these MNTNPs. In another recent investigation, Hu et al. have functionalized MSNs with polylysine-dopamine films, and rhodamine b (RhB) or DOX to make RhB/DOX@PLDA-MSNs, which have consequently displayed effective anticancer activity via enzyme-responsive-triggered-release of the drugs through the degradation of peptide bonds by the available pepsin enzymes inside the cancer cells [36]. As similar to above, Chen et al. have developed redox-responsive MSNs by conjugating them with gadolinium (Gd) based bovine serum albumin complex, and hyaluronic acid (through reductive-cleavable di-sulphide bonds) [37]. These MSNs have displayed excellent targeted drug-delivery, redox-sensitive drug-release, MRI contrast imaging via improved cell uptake by 4-T1 cells, and also enhanced cytotoxicity for antitumor suppression. Similarly, Cheng et al. have prepared redox-responsive MSNs based MNTNPs by immobilizing peptide-based amphiphile (consisting of hydrophobic alkyl-chain and hydrophilic amino-acid sequences with Tat48–60 peptide sequence having thiol termination) and RGD targeting-ligands on their surface [38]. Moreover, these MNTNPs have shown efficient loading of drug –i.e., DOX (inside the pores of MSNs) and its consecutive redox-triggered effective controlled release in the intracellular environment. Hsiao et al. have reported europium/gadolinium-(Eu^{3+}/Gd^{3+})-doped and L-cysteine (Cys)/FA-conjugated MSNs based MNTNPs for bi-modal imaging (MRI & fluorescence), tracing, and targeted cancer therapy [39]. In another analogous investigation, pH−/ultrasound-responsive, polydopamine-coated, and DOX-loaded MSNs are developed as smart MNTNPs [40]. These MSNs have effectively released the DOX (for CMT) as they are responsive to both the acidic tumor pH and applied ultrasound effects. Moreover, the MSNs have exhibited high near-IR photothermal conversion efficiency (~37%) that have effectively inhibited the growth of tumor cells via photothermal therapy. Ren et al. have reported the development of ternary-responsive MSNs by integrating them with acid−/oxidative-stress & redox-sensitive manganese oxide-coated SPIONs and camptothecin (a model cancer drug) [41]. The as-prepared MSNs have exhibited effective drug-delivery & stimuli-responsive drug-release and enhanced SPIONs/Mn^{2+} based dual T2/T1 MRI contrast inside the pancreatic cancer cells (in vitro and in vivo).

Sun et al. have prepared DOX-conjugated, Gd-doped, indocyanine green (ICG)-loaded and thermo-sensitive liposomes based MSNs as MNTNPs [42]. These MSNs have demonstrated great potentiality in cancer treatments via multimodal imaging (via NIR fluorescence imaging, photoacoustic imaging (PAI), and MRI) and also synergetic therapies (via PDT, PTT, and CMT). Recently, Yang et al. have developed perylene diimide-hybridized and ^{64}Cu-chelated photo-theranostic MSNs [43]. These MSNs have exhibited better positron emission tomography (PET) imaging functionality, and largely improved fluorescence and photoacoustic imaging capabilities (refer Fig. 2). In addition, thermo-responsive polymer growth on the hollow structure of the MSNs have increased the loading capacity of SN38-drug and its triggered/controlled release inside the cancer sites - via heat (generated via irradiation with NIR laser), which consequently helped in improving the cancer theranostic efficacies.

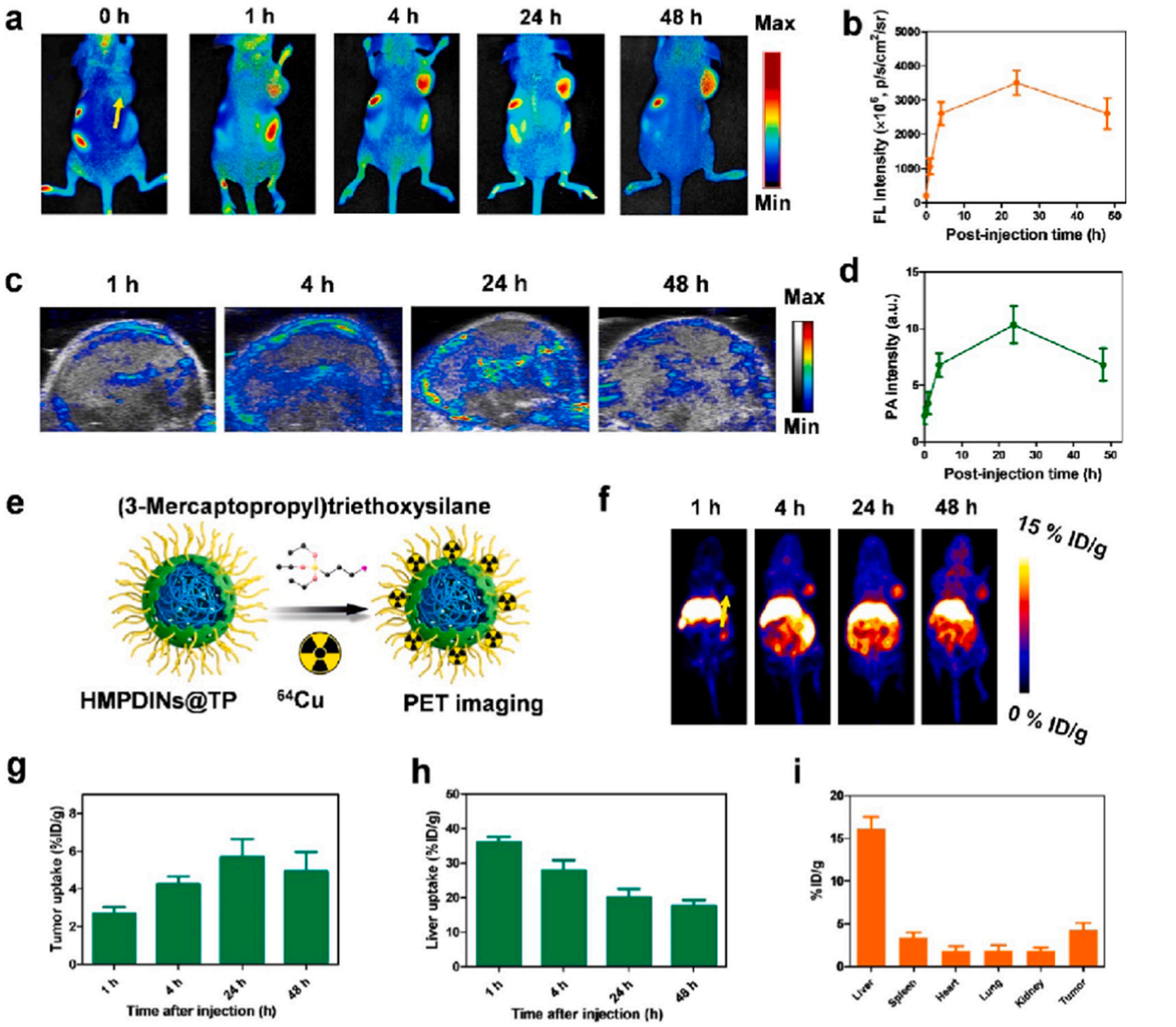

Fig. 2. In vivo FL images (a) and PA images (c) of U87MG tumor-bearing mice at various time points postinjection of HMPDINs@TP and the corresponding quantification of FL intensities of the tumor site at 700–900 nm (b) and PA intensities (d) at 760 nm of the tumor as a function of postinjection time ($n = 5$, mean ± SD) (arrow points at the tumor site). (e) Scheme of the isotope 64Cu labelling of HMPDINs@TP. (f) PET imaging for the whole-body tracking of 64Cu-labeled HMPDINs@TP (arrow points at the tumor site). (g,h) Tumor (g) and liver (h) uptakes of 64Cu-labeled HMPDINs@TP over time, as quantified by PET scans at 1, 4, 24, and 48 h postinjection (n = 5, mean ± SD). (i) Biodistribution of 64Cu-labeled HMPDINs@TP in the tumor and main organs of U87MG tumor-bearing mice at 48 h post-injection.
Adapted from Ref. [46].

2.2. Fluorescence/luminescence nanoparticles

Photoluminescence nanoparticles (PLNPs) – for e.g., lanthanide-doped upconversion NPs (UCNPs) and quantum dots (QDs) – have received substantial attention in cancer theranostics. This is because of their smaller sizes, tuneable surface functionalization, high quantum yield (QY), inherent optical/photo-physical/fluorescence properties (for instance, effective NIR absorbance & multi-colour luminescence), and real-time capability to monitor drug-delivery-cum-release for concurrent imaging & therapy [44–50]. Moreover, the instance of auto-fluorescence in the background is constricted in PLNPs (UCNPs and QDs) because of their longer emission wavelengths, which can be very much useful in deep-tissue penetration (with trivial tissue damages) [51,52]. In addition, biocompatible QDs are cadmium-free, which results in lesser cytotoxicity [53].

Recently, Dong et al. have reported extracellular-pH-specific charge-reversible NIR-based copper indium sulphide/zinc sulphide ($CuInS_2$/ZnS) QDs nanoprobe having layer-by-layer conjugation with lauric acid and 2,3-dimethylmaleic anhydride-modified ε-polylysine [54]. The as-prepared QDs have exhibited better (i) chemical stability, (ii) optical/fluorescence properties, (iii) targeting capabilities, and (iv) tumor cell uptake mediated by pH. Similarly, Song et al. have reported polyelectrolyte-mediated low-density-lipoprotein (LDL)-conjugated $AgGa_xIn_{(1-x)}S_2$ QDs fluorescence probe, which has revealed excellent biocompatibility, selective delivery, 3-D imaging, and treatment of colon cancer stem cells that overexpress the LDL receptors [55]. Liu et al. have made chromium/neodymium (Cr^{3+}/Nd^{3+}) co-doped $ZnGa_2O_4$ nanoparticles that are successful in tracking the metastasis of orthotropic breast cancer in real-time via NIR long-persistent luminescence imaging (with background-free) [56]. Moreover, the tracking via

nanoparticles has helped in imaging-guided radiotherapy (RT) that consequently resulted in the complete inhibition of metastatic breast cancer cells. In an analogous study, Ang et al. have reported better fluorescence properties (i.e., high QY of 80%) for hydrophobic oleylamine-octadecylamine ligands-coated manganese-doped zinc sulphide nanocrystals - ascribed to the promotion of diffusion of manganese atoms from the surface to ZnS crystal core by C18 ligand molecules [57]. The high fluorescence of nanocrystals has resulted in effective labelling of HeLa cells and also anti-cancer-drug delivery.

Apart from the above, UCNPs/QDs have been conjugated/functionalized with other agents/molecules to form MNTNPs to achieve multimodal cancer theranostics - a combination of distinct imaging (e.g., PET/MRI/CT) and therapeutic (PDT/PTT/RT) modalities [58–61]. For example, Yong et al. have prepared tungsten sulphide (WS_2) QDs based MNTNPs that exhibited enhanced (i) CT contrasts/PAI signals, and also (ii) multimodal image-guided therapeutic efficacy (via synergistic PTT/

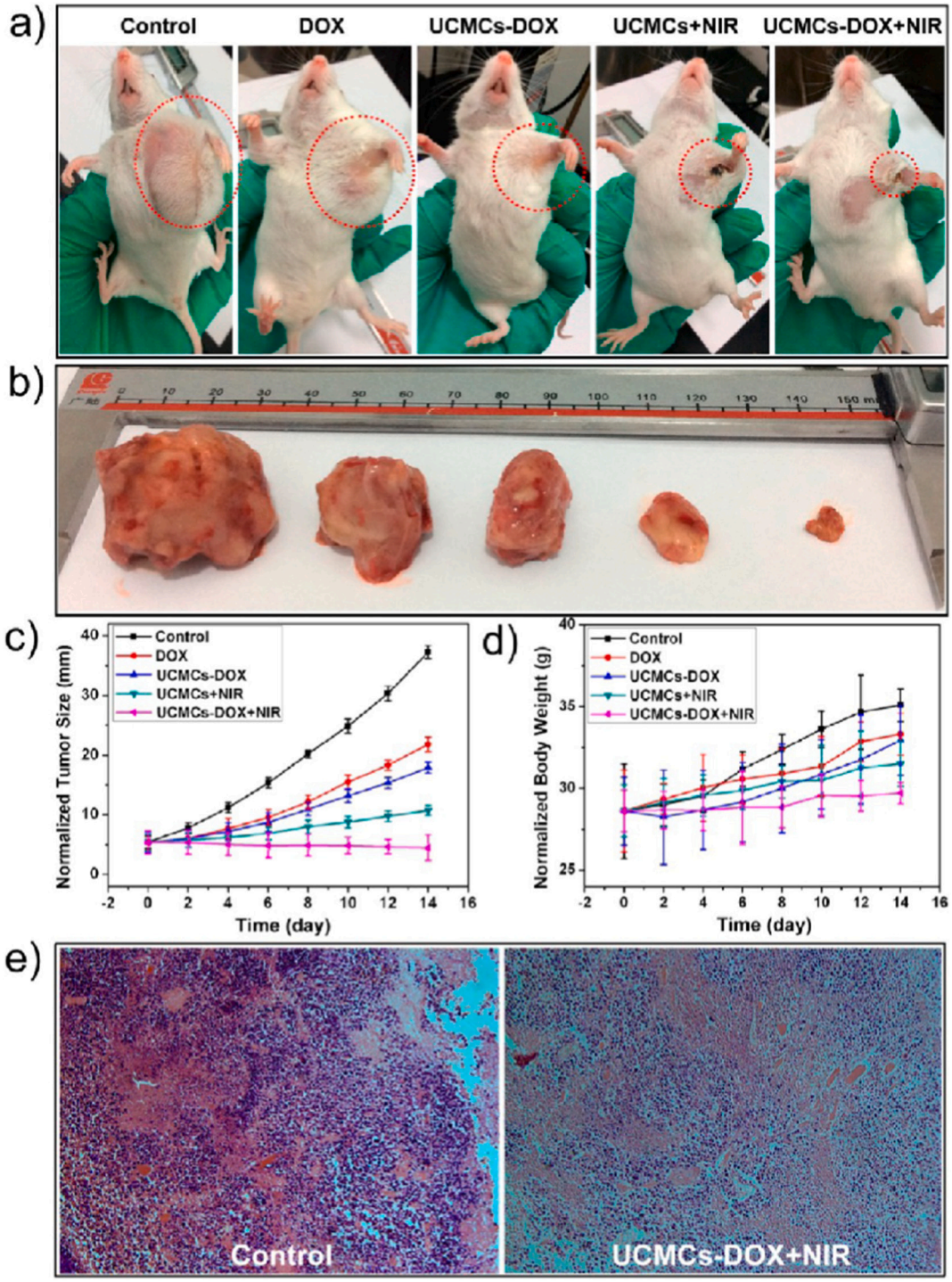

Fig. 3. (a) Representative photographs of mice after various intratumoral treatments: without anything, pure DOX, UCMCs-DOX, UCMCs under NIR irradiation, and UCMCs-DOX under NIR irradiation. (b) Photographs of tumor tissue obtained after 14 days. (c) The tumor size and (d) body weight of H22 tumor in different groups after treatment. (e) H&E stained images of tumors from the controlled group and the best treated group.
Adapted from Ref. [69].

RT effects) in in vivo tumor treatments [62]. In a similar fashion, Du et al. have prepared hybrid MNTNPs by conjugating cadmium telluride/cadmium sulphide (CdTe/CdS) QDs, DOX, and MUC1 (transmembrane glycoprotein)-targeting aptamer, which have subsequently displayed enhanced MUC1-based targeted DOX-delivery-cum-release, high cellular uptake, better fluorescence imaging and also high cytotoxicity towards MCF-7 cancer cells [63]. In another recent investigation, Guo et al. have prepared poly(acrylic acid)-coated copper hydroxide phosphate ($Cu_2(OH)PO_4$) QDs that have exhibited a strong NIR absorption, better PAI contrast, and effective PTT/PDT antitumor effects (under NIR laser irradiation) that resulted in boosted therapeutic efficacy with heightened accuracy [64]. Similarly, Wang et al. have prepared MNTNPs – made of anti-epidermal growth factor receptor (EGFR)-functionalized aminoflavone drug-loaded indium phosphate/zinc sulphide core-shell QDs [65]. These QDs based MNTNPs have been quickly uptaken by the EGFR-overexpressing breast cancer cells, which subsequently resulted in efficient tumor reduction in breast cancers that are induced in xenograft mouse models.

Recently, Lv et al. have reported GdOF:Ln@SiO_2 based MNTNPs for multimodal image-guided synergistic therapy [66]. Herein, MNTNPs are initially loaded with DOX and carbon QDs, and then conjugated with a PDT agent (ZnPc) and FA. The as-made MNTNPs have exhibited the following properties: stronger red fluorescence-emission, a large number of singlet oxygen production, and better generation of thermal effects under laser irradiation. As a result, the MNTNPs have demonstrated an increased DOX release, excellent up-conversion luminescence imaging along with MRI/CT imaging, and also enhanced therapeutic effects via CMT in synergy with PDT/PTT (under NIR irradiation), which all as a whole resulted in improved antitumor efficacy (refer Fig. 3). In another similar investigation, Qiao et al. have prepared zoledronic acid-anchored, plumbagin-loaded, and mesoporous-silica-covered pH-responsive gadolinium (III) based UPCNs, which have consequently demonstrated osteocyte (bone)-targeted early-detection and theranostic potentiality in the treatment of breast cancer bone metastasis [67].

2.3. Carbon-based nanomaterials

In the last 2 decades, different carbon-based nanomaterials (CBNs) or nano-carbons have been developed, whose types are: (i) 0-dimensional (D) fullerenes (C_{60} with hollow sphere/ellipsoid shape), 0-D nanodiamonds, and 0-D carbon quantum dots (CDs)/graphene quantum dots (GQDs), (ii) 1-D carbon nanotubes (CNTs), and (iii) 2-D graphene sheets (or graphene oxides (GO)/its derivatives - reduced GO (rGO) sheets).

Recently, scientific interests in this CBNs based nanomedicine have rapidly grown because of their unique structural morphologies, small dimensions (i.e. high surface-area-to-volume-ratio), low toxicity, biodegradability, exceptional physicochemical properties (such as stability, drug loading capacity, etc.), and versatile surface chemistry. Moreover, the functionalized CBNs (through covalent/non-covalent functionalization) have attracted enormous attention as smart DDS due to their huge potential in the cargo delivery of drugs [68]. In addition, CBNs also have high theranostic potential – as they can be efficiently used in (i) imaging because of their intrinsic two-photon fluorescence property in the NIR region, which makes them be promising in optical imaging of deep-seated tumors inside the body, and (ii) light-mediated PTT – ascribed to the better converting ability of the absorbed light into therapeutic heat [69]. Apart from the above, multifunctional CBNs (MCBNs) can be formed to provide different functionalities by combining the CBNs with distinct drugs/agents, and then functionalizing them with the targeting ligands such as vitamins, peptides, carbohydrates, proteins, etc. [70–73].

CNTs are one of the versatile CBNs that are utilized as effective contrast agents in bioimaging such as Raman imaging, NIR fluorescence imaging, and PAI – attributed to their unique optical properties [74]. In addition, CNTs have extraordinary optical absorbance capability both in the visible/NIR region, which is useful in inducing heat by converting the light, thus permitting the CNTs to be applied as active PTT agents in cancer treatments. CNTs are normally synthesized by heating carbon-black & graphite in an organized flame environment. However, high-quality/pure CNTs with controlled sizes/shapes and properties can be synthesized only via chemical vapour deposition or laser ablation methods. Types of CNTs include single-walled CNTs (SWCNTs) and multi-walled CNTs (MWCNTs)). Although MWCNTs can cross biological barriers, SWCNTs are commonly used in cancer theranostics – owing to their (i) well-defined walls and smaller structural defects, and (ii) solubility (biodistribution) and ability to get localized in selective cellular compartments via proper surface functionalization such as PEGylation [75–78]. Moreover, functionalized CNTs (SWCNTs/MWCNTs) can be efficiently utilized as DDS/nanocarriers to effectively deliver molecules such as anti-cancer drugs, peptides, antigens, and nucleic acids inside the cancer cells, and also they can be exploited as multifunctional cancer nanomedicines (i.e., MNTNPs) [79–81]. Recently Sobhani et al. have demonstrated a substantial decline in melanoma tumors in cancerous mice via PTT (exposing to NIR irradiation for 10 mins) by using PEGylated oxidized-CNTs (O-CNT-PEG) [82]. Similarly, Zhao et al. have reported polydopamine (PDA)-coated and PEGylated SWCNTs as MNTNPs for use in multimodal imaging (MRI and nuclear (gamma) imaging) by labelling them with a radionuclide (^{131}I) and chelating with Mn^{2+} ions (which acts as both T1 & T2 MRI contrast agents) [73]. Moreover, these SWCNTs have revealed an outstanding synergistic antitumor therapeutic efficacy (via radio-nuclide therapy and PTT) and effective in vivo tumor accumulation after systemic administration into mice. In an analogous fashion, Dong et al. have developed a transactivator of transcription (TAT)-chitosan-functionalized MWCNTs as a promising nanocarrier for faster and sustained drug release of DOX under lower pH conditions, which have enhanced the anti-tumor efficacy in hepatoma (BEL-7402) induced mice when performing CMT in combination with PTT [83]. Besides, Li et al. have reported oxidized-single-walled-carbon-nanohorns (OxSWNHs) as a potential nanocarrier to deliver a large amount of chemo-drug (vincristine (VCR)) to the tumor sites via active targeting (monoclonal-antibodies (mAb)-functionalization) for effective therapeutics in tumor-bearing mice models with less toxic effects towards normal tissue [84]. Moreover, in this work, OxSWNHs have revealed 80% cumulative/sustained release of chemo-drug. In another study, Ryu et al. have made FA (for active targeting)-conjugated nanodiamonds to simultaneously perform PTT and optical imaging of tumor tissues in a selective manner [85].

GO/rGO can also produce PTT heating effects via photon-to-thermal-energy transfer, on exposure to NIR irradiation. In a recent study, Kalluru et al. have demonstrated GO-based in vivo multicolour fluorescence cancer imaging in visible/NIR region [86]. Herein, GO is functionalized/conjugated with PEG/FA to achieve GO-PEG-folate-mediated active targeting, which has resulted in better PDT/PTT effects upon NIR irradiation (980 nm) that further minimized the growth of induced-melanoma-(B16F0)-tumors in mice models. Lately, Liu et al. have prepared Fe_3O_4 embedded−GO based TNPs, which have showed higher bioimaging efficacies (via MRI/CT) and heating efficiency (via MHT) [87]. In another investigation, Chen et al. have reported biocompatible and photo-responsive rGO/carbon/MSN nanocarriers for NIR-triggered synergic photo-chemo-thermal therapy (refer Fig. 4), where the results have displayed a substantial reduction in the size of MDA-MB 231 tumors in mice within 14 days of treatment [88]. Likewise, Hu et al. have developed rGO based theranostic nanomedicines by functionalizing a significant amount of ICG fluorescence molecules on the surface of PDA-coated rGO [89]. This ICG-functionalized-PDA-rGO based TNPs have revealed robust PTT effects (by completely suppressing 4 T1 tumor growth) and higher PAI contrast, without generating any toxic effects to the normal healthy cells. In an analogous investigation, Imani et al. have prepared dual-functionalized (i.e., phospholipid-based-amphiphilic-polymer and R8-cell-penetrating-peptide (CPPs))-rGO based nanocarrier for delivering therapeutic siRNA, which have consequently

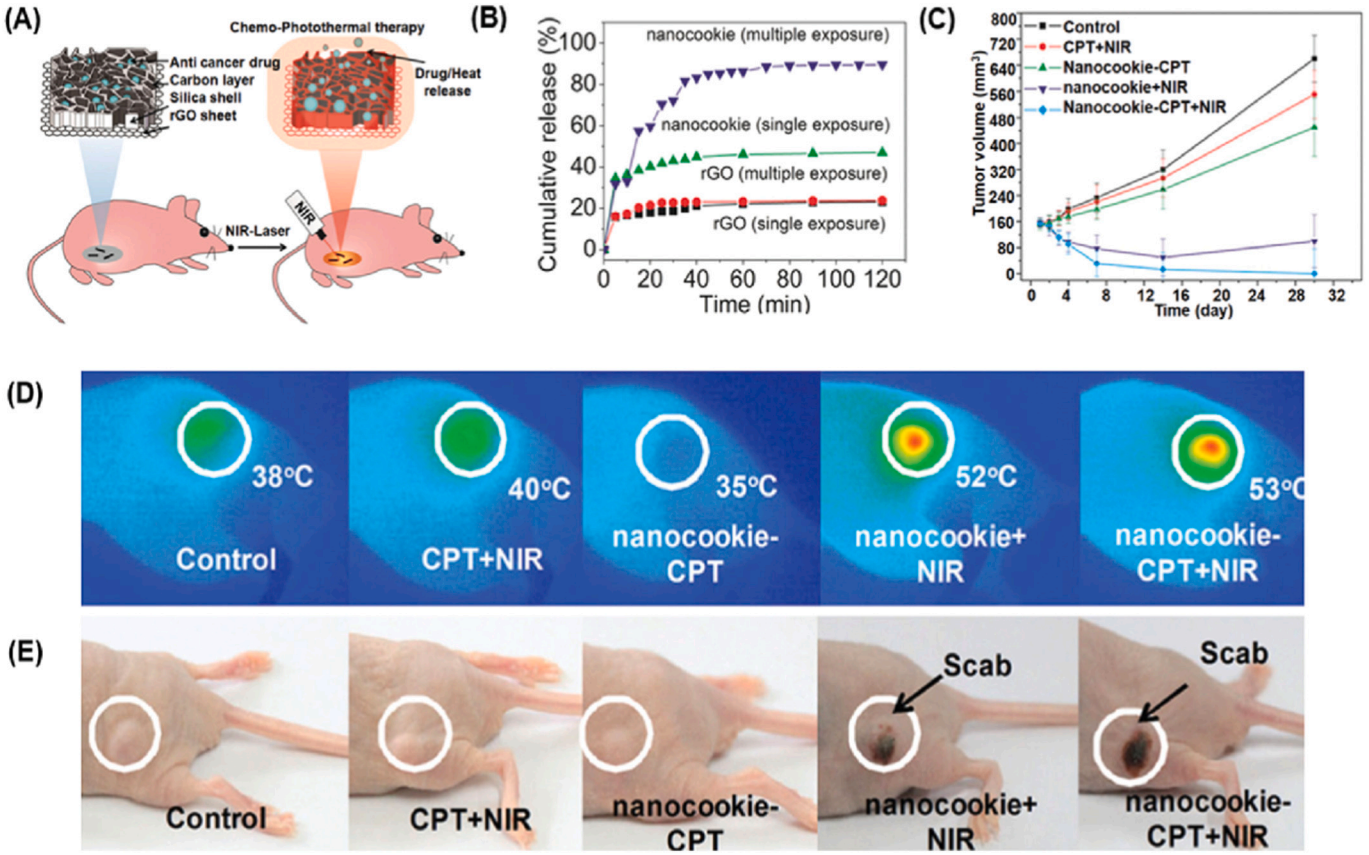

Fig. 4. NIR-induced combined PTT/CMT and optical imaging with rGO-based nanocookies for tumor treatment. (A) Schematic illustration of chemo/photothermal therapy using rGO/carbon/mesoporous silica nanocookies under NIR light-control. (B) NIR-stimulated drug (CPT) release profiles from rGO and nanocookies: single 5 min NIR exposure initiated at time 0, multiple exposures repeated 5 times after 5 min waiting time following previous exposure. (C) Tumor volume change with PBS + NIR (control), CPT + NIR, nanocookie-CPT (no NIR), nanocookie + NIR, nanocookie-CPT + NIR. (D) Infrared thermal image of PBS + NIR (control), CPT + NIR, nanocookie-CPT (no NIR), nanocookie + NIR, and nanocookie-CPT + NIR treatment. Colour bar on the right shows the temperature in degrees Celsius. (E) At day 4 after NIR irradiation (808 nm, 0.75 W cm_2, 5 min, 1 min interval for every min treatment). Tumor turned into a scab at the sites injected with nanocookie + NIR and nanocookie-CPT + NIR.
Adapted from Ref. [89].

exhibited excellent gene silencing ability, higher internalization efficiency, and substantial MCF-7 cancer cell growth inhibition [90]. Similarly, Zhang et al. have established rGO based theranostic nanoplatform by functionalizing it with Ru(II)-complex-modified-PEG via π-π stacking/hydrophobic-interactions [91]. Functionalized rGO has revealed effective in vivo cancer PTT/PDT treating effects through apoptosis induction (via reactive oxygen species (ROS) and cathepsin-based signaling pathways) on excitation with 808/405 nm laser.

Ge et al. have reported biocompatible, photo- and pH-stabile GQDs with higher QY (~1.3), which have permitted simultaneous visible-light activated imaging and PDT (via singlet oxygen generation) treatment of tumor tissues [92]. GQDs have also enhanced the CMT efficacy of the cisplatin by increasing its cellular uptake by improving the cell penetrability and then supporting its interactions with DNA [93]. Thakur et al. have reported multifunctional GQDs based theranostic nanocomplex for concurrent cancer imaging and drug delivery [58]. Initially, GQDs are conjugated with an anti-cancer drug (berberine hydrochloride) through cysteamine hydrochloride (Cys) to develop a nanocomplex, which has exhibited high drug loading efficiency (88%), improved biocompatibility, multi-excitation based cellular imaging, and significant cytotoxic effects in different cancerous cell lines. Similarly, Iannazzo et al. have covalently linked GQDs with biotin targeting molecules for improving the cellular uptake in biotin-receptor-overexpressed-tumor cells and also loaded with DOX for its targeted delivery inside cancer cells [94]. Alike, De et al. have formed DOX-loaded and FA-conjugated chitosan-functionalized GQDs based nanocarrier, which further have exhibited tumor-specific DOX-delivery with enhanced therapeutic efficacy in A549 cancer cells through higher drug release at lower pH 5.5 [95].

CDs (a new family member of CBNs) are spherical, nontoxic, and discrete particles with sizes less than 10 nm. CDs have outstanding photoluminescence, superior electron transfer ability, and adaptable surface engineering behaviours, hence they have attracted significant attention in bioimaging field as a new generation fluorescent nanoparticles in recent years. Lately, CDs have also been explored as PTT/PDT heating agents also, as they can produce localized heat by converting NIR light to thermal energy at the tumor sites, for effective cancer therapy. Recently, Singh et al. have reported bioactive CDs that displayed strong multi-colour luminescence with high photo-stability, NIR-based PTT effects, high DOX loading (90%) and delivery, and pH/NIR-controlled DOX release [96]. Similarly, Ge et al. have demonstrated image-guided concurrent PDT/PTT therapeutics and fluorescence imaging via biocompatible and photo-stable CDs-based theranostic agents (refer Fig. 5) [97]. In this work, well-dispersed CDs with different sizes (6–10 nm) are prepared by using polythiophene benzoic acid (Fig. 5A and B), which emitted red-light on excitation. These CDs have produced singlet oxygen species ($^1O_2$) and heat simultaneously under laser irradiation (Fig. 5C) in respective PDT and PTT cancer treatments, which are confirmed by the in vitro and in vivo images (Fig. 5D and E). Likewise, Jia et al. have reported self-assembling NIR-responsive CDs based photo-sensitizers, which have demonstrated effective simultaneous NIR activation/fluorescence imaging and also

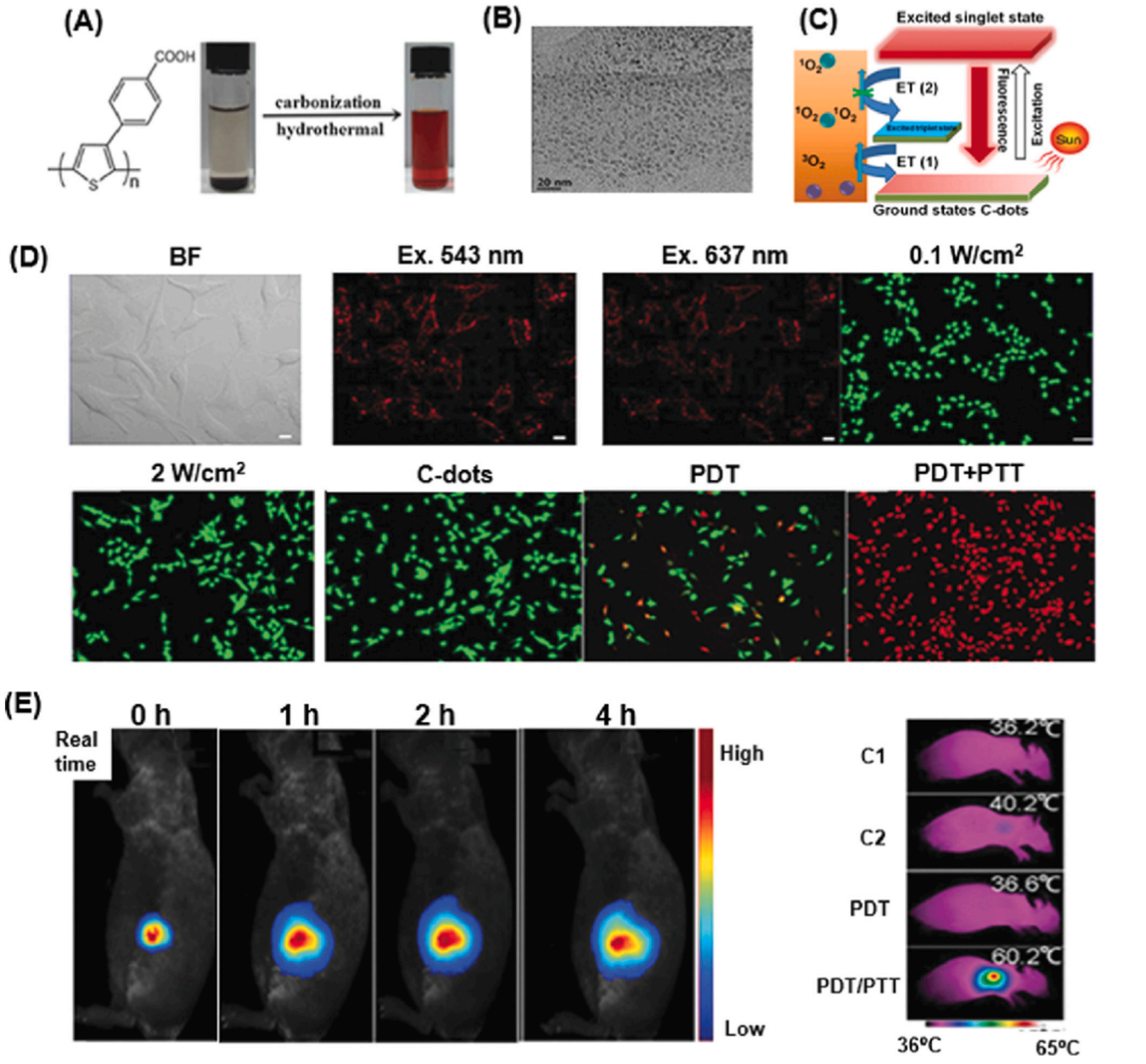

Fig. 5. C-Dot-based combined PDT/PTT with bioimaging. (A) Fabrication of C-dots. (B) TEM image of C-dots. (C) Mechanism for the single oxygen 1O2 generation by C-dots. (D) In vitro imaging and PDT/PTT with cancer cells. (E) Fluorescence images of calcein AM/PI-stained cancer cells with laser irradiation; 635 nm laser at power densities of 0.1 W cm_2 (PDT) and 2 W cm_2 (PDT/PTT) for 10 min. (F) In vivo real-time fluorescence imaging and photothermal imaging with PDT/PTT. Adapted from Ref. [101].

PDT therapy (under laser irradiation) in in vitro and in vivo environments [98]. Similarly, Kajani et al. have reported green and facile one-pot hydrothermal synthesis process for preparing highly photo-stable and photo-luminescent (multi-colour) hexagonal shaped CDs by combining Taxane with diamines [98]. The as-prepared CDs have exhibited narrow size distribution, high QY (up to 50.4%), and better anti-cancer activities by inducing apoptosis-mediated cell death. Very recently, Scialabba et al. have used a facile and flexible method to prepare monodispersed PEGylated and biotinylated multifunctional CDs [99]. These CDs have exhibited (i) better loading of a great amount of anticancer drugs (16–28% Irinotecan) and targeted drug-release/cell-internalization, and also (ii) strong fluorescence imaging along with higher NIR-triggered localized heat for inducing effective cancer cell death.

2.4. Metal nanoparticles

Metallic nanoparticles (MEPs) have attracted considerable interest in biomedical fields – mainly ascribed to their small size (for easy adsorption/absorption/penetration), large surface area, facile synthesis of various shape, high cargo loading capacity (ability to deliver drugs, DNA, etc.), higher intercellular uptake, unique optical properties (surface plasmon resonance, SPR, etc.), and versatile functionalization [100–103]. In recent years, MEPs particularly Au, Ag, and Pt NPs have been largely on focus for cancer theranostics due to their inherent CT, PA, fluorescence, and surface-enhanced Raman scattering (SERS) imaging properties and PTT capabilities [104–108]. However, the surface of the MEPs are modified (e.g. PEGylated) to improve their biocompatibility and overcome RES uptake [109,110]. Moreover, MEPs are functionalized with tumor-specific ligands or stimuli-responsive

components and conjugated with other therapeutic/imaging agents to accomplish targeted/triggered delivery and multimodal cancer theranostics [111–115].

2.4.1. Silver nanoparticles

Silver (Ag) nanoparticles possess remarkably superior (i) physicochemical properties including high thermal conductivity, better plasmonic properties, & chemical stability, and (ii) high anti-bacterial/−viral/−fungal, and antioxidant properties [116,117]. Ag nanoparticles are widely utilized in different applications including cancer (i) diagnostics/imaging, (ii) therapeutics (via any one of the following: revoking cell cycle, the formation of micronuclei, discharging lactate dehydrogenase (LDH), ROS production, generation of apoptotic genes (for e.g. Bax), and bringing DNA-damages/chromosomal aberration) and (iii) drug delivery [118], where Table 1 shows important Ag nanoparticles used in cancer imaging and therapy. For example, Swanner et al. have functionalized Ag nanoparticles with a fluorescent moiety cyanine3 attached to PEG5000-thiol (Cy3-PEG5000-SH) in a reliable/reproducible manner to image 2D and 3D tumor models [119]. This tumor imaging has provided effective insights into the cellular localization of nanoparticles, and their diffusion through a tumor spheroid. In an analogous investigation, Wu et al. have formed PEG-1-butyl-3-methylimidazolium hexafluorophosphate (IL, microwave sensitizer)/zirconium oxide (ZrO_2)-Ag@silica (SiO_2) nanorattle, which are effectively used in CT imaging-guided concurrent microwave-based thermal therapy for H-22 tumor treatment [120].

In the case of therapeutics, size−/shape−/surface chemistry-based anti-cancer activities of Ag nanoparticles have been investigated. However, the concentration (or) dose-dependent anti-cancer therapeutic activity of Ag nanoparticles is widely studied. For instance, Naz et al. have reported dose-dependent anticancer activity for Ag nanoparticles (5–20 nm, prepared via seed extracts of *Setaria verticillata*) against breast cancer – i.e., MCF7-FLVcells [121]. Moreover, these nanoparticles are loaded with anti-cancer drugs such as DOX and daunorubicin (DNR) for their delivery inside leukemia cells for their treatment via CMT. Similarly, the plant-derived Ag nanoparticles – i.e., from potentilla fulgens, G. neojaponicum [122], dimocarpus [123], starch [124], artemisia princeps [125], and *Origanum vulgare* [126] are used in the treatment of respective cancers such as MCF-7, MDA-MB-231, PC-3, HCT116, L132, and A549 cells. In an analogous study, Jadhav et al. have performed phytosynthesis of Ag nanoparticles by using the aqueous extract derived from the plant - *Salacia chinensis* [127]. Herein, the green synthesized Ag nanoparticles have shown (i) biocompatibility towards normal human fibroblasts & blood erythrocytes, and (ii) cytotoxicity against PC-3, HepG2, KB, L-132, HeLa, and MDA-MB-231 cancer cell lines.

In an analogous investigation, Liu et al. have evaluated the therapeutic-effects of Ag nano-triangles combined with five various CMT drugs (cyclophosphamide (CTX), gemcitabine (GEM), 5-fluorouracil (5-FU), oxaliplatin (OXA), and DOX) against different breast cancer cell lines (MDA-MB-231/MCF-7/4 T1 cells) based on the induced ROS levels after the exposure to Ag nanotriangles, cancer-drugs or their combination [128]. Herein, the results have showcased that the synergism of Ag nanotriangles with CTX/GEM can be type–specific in breast cancer treatment. But, the other drugs – i.e., 5-FU/OXA/DOX have displayed stronger synergistic anticancer effects in combination with Ag nanotriangles in all tested cancer cell lines.

In drug delivery, recently Qiu et al. have prepared an exclusive DDS - made of Ag nanoparticles that are loaded with camptothecin (CPT, an anti-cancer drug)-based polymer-prodrug, wherein the drug is associated with the side chains of the polymer through acid-cleavable β-thiopropionate bonds as shown in Fig. 6 [129,130]. Here, the authors have taken advantage of the "ON" and "OFF" characteristics of the Ag nanoparticles-based nanoparticle surface energy transfer (NSET) effect to vividly track the drug release, where the characteristics are dependent on the distance change between CPT and Ag nanoparticles.

Table 1
Important Ag & Au nanomaterials for cancer imaging and therapy.

Type of nanomaterials	Surface modification/drug loading/conjugation in nanomaterials	Comments	Ref
Ag	Cyanine3 (Cy3)-PEG5000-SH modified Ag nanoparticles	Insights on cellular localization of Ag nanoparticles, & their diffusion through a tumor spheroid	[123]
	PEG-1-butyl-3-methylimidazolium hexafluorophosphate (IL, microwave sensitizer)/zirconium oxide (ZrO_2)-Ag@silica (SiO_2) nanorattles	CT imaging-guided concurrent microwave based thermal therapy for H-22 tumor treatment	[124]
	Setaria verticillata seed extract based Ag nanoparticles loaded with doxorubicin (DOX) and daunorubicin	MCF7-FLV and leukemia cancer cells treatment	[125]
	Ag nano-triangles with five different chemotherapy drugs - cyclophosphamide (CTX), gemcitabine (GEM), 5-fluorouracil (5-FU), oxaliplatin (OXA), and DOX	MDA-MB-231, MCF-7, and 4 T1 cancer cells treatment	[132]
	Camptothecin (CPT) laoded Ag nanoparticles based polymer-prodrug	CPT drug release studies	[134]
	Chitosan-coated Ag-gadolinium nano-alloy (AgGd) based bimetallic nanoparticles (BNPs) loaded with DOX	CT/MRI imaging and cancer therapy	[174]
	Chitosan-coated DOX-loaded Ag-dysprosium (Ag—Dy) BNPs	CT/MRI imaging and HeLa cancer cell treatment	[175]
Au	Hyaluronic acid-functionalized siRNA based HSP72-targeted Au nanostars	Imaging of CD44-overexpressed triple negative breast cancer cells	[137]
	Plasmonic Au nanostars with cyclic arginine-glycine-aspartic acid (cRGD) peptides	Photoacoustic imaging of tumor angiogenesis	[138]
	Glycol chitosan (GC) or Heparin molecules functionalized Au nanoparticles	CT imaging of colon cancer-bearing mice	[139]
	PEGylated polyethyleneimine (PEI)-entrapped Au nanoparticles	Blood pool CT imaging	[140]
	PEI-stabilized Au nanoparticles	CT contrast agent for imaging of (i) blood pool and major organs of rats, (ii) lymph node of rabbits, and (iii) xenografted tumor model of mice	[141]
	PEI modified plasmonic Au fractal nanoaggregates	photoacoustic imaging and photothermal therapy in an animal model with colorectal carcinoma	[142]
	6-thioguanine attached Au nanoparticles	Anti-cancer activity in breast cancer (MCF7) cell line	[146]
	Apolipoprotein E modified Au nanorods attached with chlorin e6 (Ce6) molecules	Photothermal and photodynamic therapies in Cal-27 oral squamous cell carcinoma cells	[269]
	PEI-entrapped folic acid (FA)-targeted Au nanoparticles chelated with gadolinium (Gd)	Dual-modal imaging (CT and MRI) of tumors	[180]

(*continued on next page*)

Table 1 (*continued*)

Type of nanomaterials	Surface modification/drug loading/conjugation in nanomaterials	Comments	Ref
	Au nanospheres attached with cyptate (Cy - indocyanine green based an NIR fluorophore) through urokinase-type plasminogen activator (uPA - a breast cancer enzyme) enzyme-substrate-motif (G-G-R)	Fluorescence visualization and hyperthermic killing of breast cancer cells	[183]
	Anti-human epidermal growth factor receptor 2 (Her2) antibodies-conjugated Au-nanoshelled poly(lactic-co-glycolic acid) magnetic hybrid nanoparticles	Contrast-enhanced ultrasound imaging & T2-weighted MR imaging and photothermic killing of SKBR3 cancer cells	[185]
	PEI-PEG modified, glioma-specific peptide (chlorotoxin, CTX) and 3-(4-hydroxyphenyl) propionic acid-OSu (HPAO) entrapped Au nanoparticles with iodine radiolabelling	Single-photon emission computed tomography/CT imaging and radionuclide therapy of glioma cells	[186]

2.4.2. Gold nanoparticles

As similar to Ag nanoparticles, Gold (Au) nanoparticles are extensively used in various single-modal theranostic applications (with targeting functions) including optical−/photoacoustic-/CT-imaging of cancer cells, PTT, and delivery of anti-cancer drugs, since these nanoparticles display tunable physicochemical properties (by having different size (2–100 nm) shapes including nanospheres, nanorods, nanoshells, nanocages, and nanostars), surface plasmon resonance (SPR - reaching of maximum oscillation amplitude at a definite frequency) based optical properties and also tailor-made surface-functionalization [131,132]. For example, in a recent study, Wang et al. have prepared hyaluronic acid-functionalized siRNA against HSP72-targeted Au-nanostars and effectively observed CD44-overexpressed triple-negative breast cancer (TNBC) cells under dark-field optical microscopy [133]. In another investigation, Nie et al. have prepared cyclic arginine-glycine-aspartic acid peptides-functionalized plasmonic Au-nanostars which have resulted in efficient photoacoustic imaging of tumor angiogenesis, since these functionalized nanostars have displayed high affinity towards integrin αvβ3 overexpressing tumor neovessels [134]. Similarly, Sun et al. have altered the surface of Au nanoparticles using biocompatible glycol chitosan (GC) molecules and compared their CT contrast behavior with that of heparin-molecules-modified Au nanoparticles to realize GC as a targeting molecule in colon cancer-bearing mice [135]. The CT cross-sectional image results have revealed that HEPA-based Au nanoparticles are accumulated in the spleen and liver, whereas most of the GC-based counterparts are inside the tumor, which confirmed the targeting affinity of GC towards cancer. Analogously, Zhou et al. have prepared water-soluble polyethylene glycol (PEG) coated (PEGylated) polyethyleneimine (PEI)-entrapped Au nanoparticles with tuneable core sizes (ranging from 1.9–4.6 nm) [136]. These nanoparticles demonstrated (i) superior X-ray attenuation properties as compared to Omnipaque (an iodinated clinical contrast agent) and also (ii) competent and boosted blood-pool CT imaging (up-to 75 min) – attributed to the extended half-decay time of 11.2 h.

In another similar investigation, Zhang et al. have reported the design & development of PEGylated and branched-PEI-functionalized Au nanoparticles [137]. Herein, the nanoparticles have displayed efficient CT contrast, which have enabled the effective imaging of (i) blood-pool/major organs of rats, (ii) lymph-nodes of rabbits, and also (iii) xenografted mice tumor models. Moreover, the nanoparticles have displayed excellent in vivo stability and are shown to be excreted out within the designated time. In another research study, Mulens-Arias et al. have created Au nanoparticles via PEI-assisted method, where these nanoparticles are self-arranged in a controlled manner and have resulted in obtaining NIR-absorbent plasmonic fractal nanoaggregates [138]. These nanoaggregates have demonstrated high diagnostic (via PAI) and therapeutic (PTT) efficiency in animal models induced with colorectal carcinoma. Similarly in another investigation, glucose conjugated Au nanoclusters (AuNCs) are prepared by Cheng et al. to perform cancer-target imaging/probing of overexpressed glucose transporters in U-87 MG cancer cells, based on the glucose cleaving by glycotic enzymes [139]. In a similar fashion, Zhu et al. have synthesized polymer PDPP-DBT-conjugated and antimicrobial peptide (AMP - Tachyplesin-I)-loaded AuNCs for the effective and step-wise killing of HT-29 cells through photothermal ablation by irradiating NIR light (at 808 nm) for 5 min [140]. Similarly, Wang et al. have made Herceptin-conjugated bovine serum albumin (BSA)-protected AuNCs for site-specific targeting of ErbB2 over-expressing SK-BR3 (breast cancer) cells and tumor tissues and also consequent nuclear localization, where the results have indicated that the localization effect has enhanced the antitumor efficacy by inducing massive DNA damage [141].

Apart from the above, Chen et al. have used Au nanoparticles as drug carriers to deliver methotrexate (MTX, a chemotherapeutic drug) via functionalization through carboxyl groups (–COOH) [142]. Herein, MTX accumulation is faster and also higher inside the tumor cells that are treated with drug-attached Au nanoparticles than that of free MTX. Moreover, drug-bound nanoparticles have shown improved cytotoxic effects in cancer cell lines, and also have suppressed the growth of tumor in a mouse ascites model of Lewis lung carcinoma, whereas an equivalent free drug dose has no anti-tumor effects. In another similar investigation, Karimi-Maleh et al. have delivered an anti-cancer drug 6-thioguanine by attaching this thiolic drug on the surface of Au nanoparticles and consequently accomplished heightened anti-cancer action in breast cancer (MCF7) cell lines [143]. In an analogous study, Mondal et al. have packed Au nanoparticles on hydroxyapatite surface, which is further modified with collagen to successfully load and deliver DOX [144]. Similarly, Zhu et al. have constructed a multifunctional dendrimer-based theranostic system, where DOX is primarily covalently linked onto the partially acetylated generation 5 poly(amidoamine) based dendrimers [145]. The dendrimers are functionalized with FA via acid-sensitive cis-aconityl linkages and are made to entrap Au nanoparticles. These entrapped nanoparticles have effectively achieved combined cancer cell CT imaging and CMT with high targeting specificity. In another recent study, Yeo et al. have formed a homogeneous protein corona around Au nanorods using apolipoprotein E [146]. Through corona, hydrophobic photosensitizer molecules - chlorin e6 (Ce6) are loaded on the surface of the nanorods and successfully delivered in higher amounts inside Cal-27 oral squamous cell carcinoma cells. In addition, ~96.7% of cancer cells are killed via combined photothermal therapy (through the nanorods) and PDT (with 2 μM loaded Ce6 molecules). In a similar fashion, the Au nanoparticles are investigated for their diverse use in stand-alone imaging, therapy, and drug delivery [103,131,147–149].

In addition to the above, Au nanoparticles are more useful in simultaneous cancer therapy and diagnostics (theranostics). For instance, Vickers et al. have synthesized hollow Au nanospheres - utilized mainly in 2-photon imaging and PTT of cervical cancer, where deep-tissue-penetrable NIR (having wavelength of 650–950 nm) is used as a trigger for imaging and therapy [150]. Moreover, the FA − PEG−thiol molecules-based bio-functionalization onto hollow Au nanospheres has effectively improved the binding of these nanospheres towards FA-overexpressing HeLa cells, thereby enhancing the cancer theranostic efficacy. In a similar investigation, Wang et al. have prepared a different kind of bio-orthogonal Raman reporter/aptamer (AS1411/MUC1)-functionalized Au nanorods for both SERS imaging

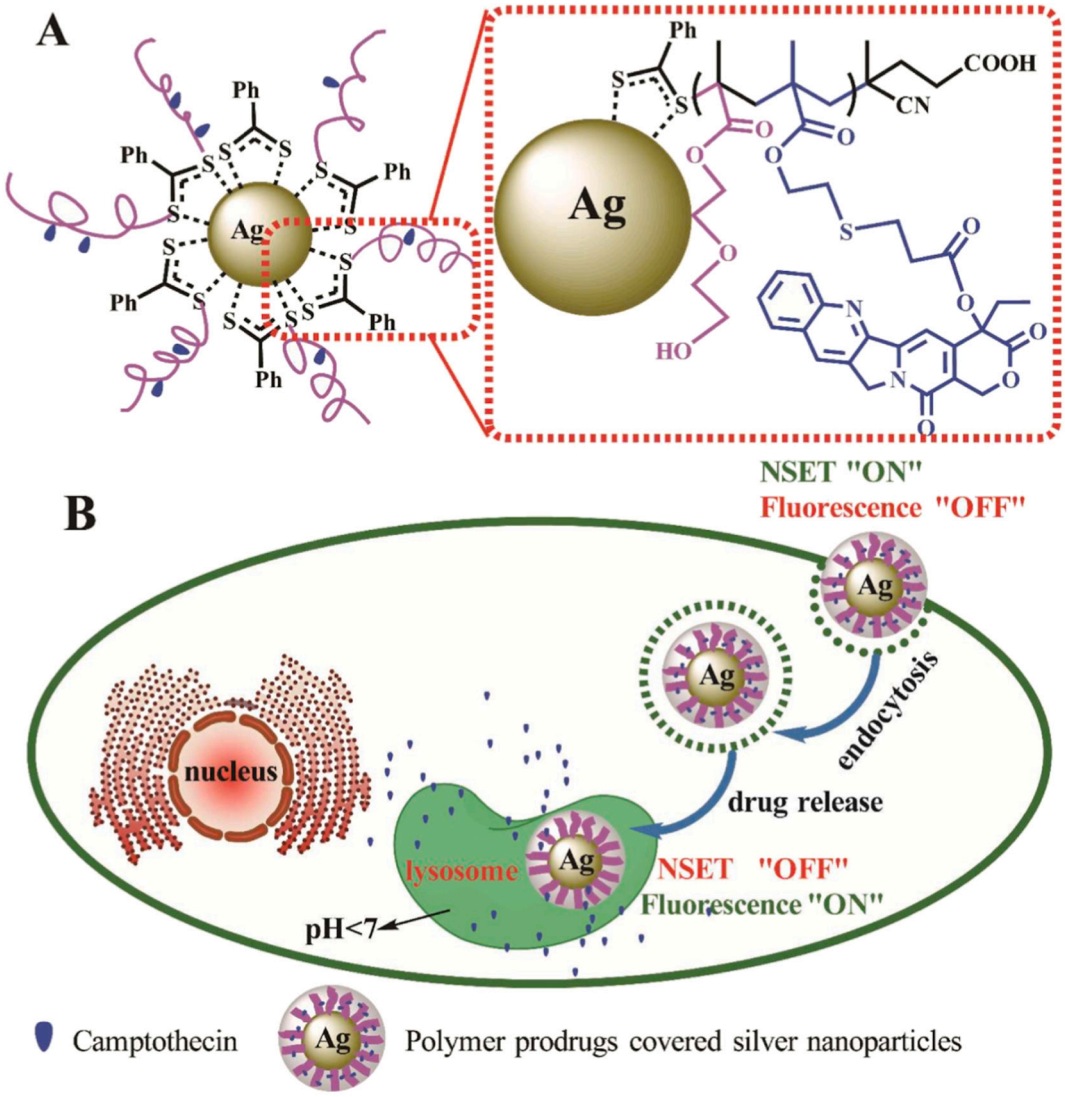

Fig. 6. Schematic illustration of the polymer prodrugs-covered Ag nanoparticle (A) and intracellular release process of camptothecin CPT (B). The fluorescence of CPT is quenched when it is linked to the polymer chain on the surface of AgNPs (NSET "ON" or Fluorescence "OFF"), while the CPT fluorescence is recovered (NSET "OFF" or fluorescence "ON") when it is released with response to cellular acid conditions.
Reproduced with permission from Ref. [134].

and PTT [151]. Herein, Au nanorods have exhibited a strong Raman signal (i.e., at 2205 cm^{-1}) in the biological Raman-silent region, which is utilized for identifying MCF-7 breast cancer cells through Raman imaging. Moreover, laser irradiation (808 nm / 1 W/cm^2) for only 10 mins inhibited almost 99% of MCF-7 cancer growth in tumor-bearing nude mice, which is ascribed to enhanced accumulation of Au nanorods via aptamer functionalization.

Analogously, Li et al. have utilized dye (TRAMA)-loaded PcPp peptide (including capping peptide Pc ($GGGGGLVPEGSCCYNH_2$) and probe peptide Pp (CCYGGGGRGRK (FITC)GNH_2))-conjugated ultra-small gold nanoclusters (AuNCs) to perform imaging of caspase-indicated cell apoptosis in real-time through NSET–based fluorescent probing [152]. Herein, the activation of intracellular caspase 3 (through the cleaving of peptides in NCs) has led to the release of the dye resulting in the continuous monitoring of its activity in a living cell, and also consequent induction of the therapeutic apoptosis process as shown in Fig. 7. In another analogous investigation, AuNCs are synthesized through (deoxy guanosine 5′-triphosphate (dGTP)-template, then formed a complex by conjugating with cisplatin and finally covered with PEG for theranostic treatment of HeLa cells [153]. In a similar study, Dutta et al. have prepared phenylboronic acid (PBA) template AuNCs for detection of mucin biomarker and also targeted-imaging of HeLa and HepG2 cancer cells in in vitro conditions along with certain therapeutic effects via PBA [154]. In a recent investigation, Ghoshal et al. have loaded AuNCs with secreted frizzled-related protein 1 (SFRP1) to focus on the up-regulated pathway in the cancer cells for enhancing their anti-proliferation by the surface-attached cisplatin drug [155]. Moreover, the AuNCs are exploited for utilization in binding and consequent imaging of the cancer cells. Similar AuNCs based nano-systems are utilized in theranostics of different cancer cells [156–159]. Table 1 shows significant Au nanoparticles for cancer theranostics.

2.4.3. Other metal nanoparticles

Apart from Ag & Au, there are other metals/metallic nanoparticles-for e.g., copper (Cu), platinum (Pt), titanium (Ti), bismuth (Bi), and so on – that are utilized in cancer imaging and therapy [160,161].

For example, Goswami et al. have prepared transferrin-templated blue-luminescent Cu nanoclusters (Tf-Cu NCs) that are electrostatically loaded with DOX on their surface [162]. Herein, Förster resonance energy transfer (FRET) within Dox-loaded NCs has shown red-

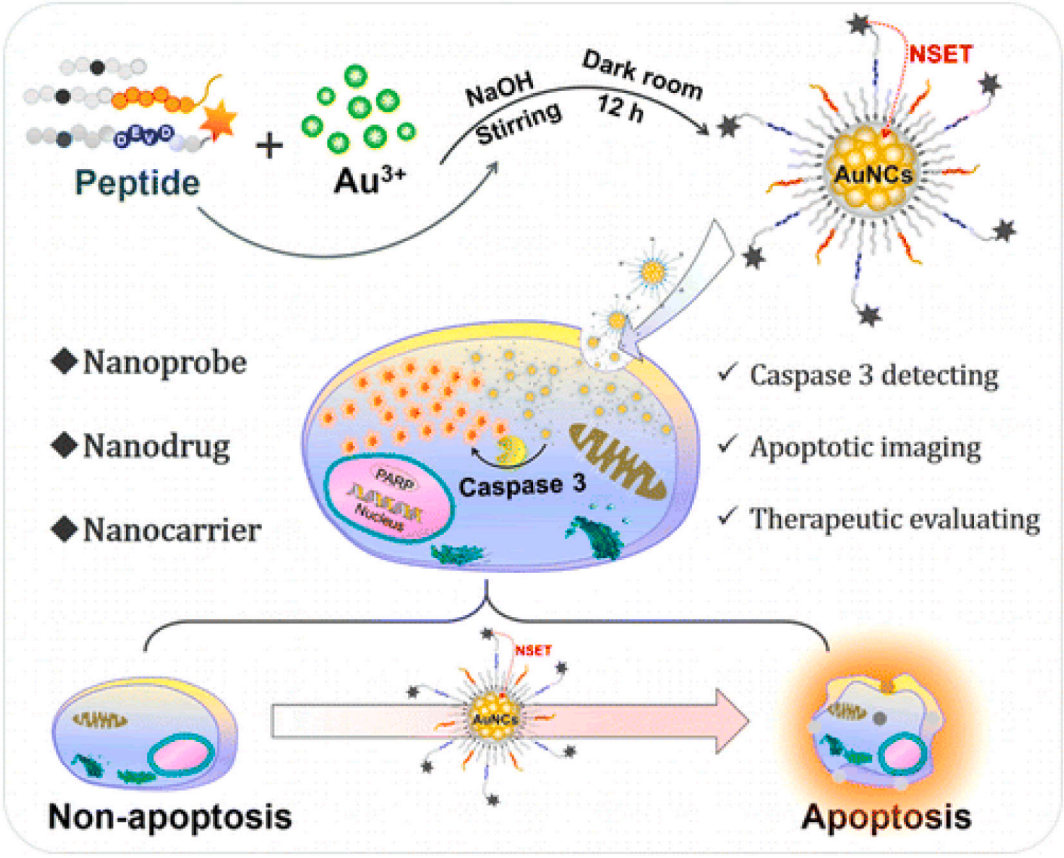

Fig. 7. Schematic illustration of AuNCs-Based Nanoprobe for real-time imaging of caspase-indicated cell apoptosis through nanosurface energy transfer (NSET)–based fluorescent probing.
Reproduced with permission from Ref. [156].

luminescence, while quenching the blue-luminescence of NCs. However, after the internalization via overexpressed Tf receptors, the blue-luminescence of Dox-loaded Tf-Cu NCs has been re-established in the cytoplasm, whereas the red-luminescence is occurred in the nucleus of cancer cells (HeLa & MCF-7) due to the migration of DOX. In addition, high therapeutic efficacy is also obtained – i.e., better tumor inhibition in Dalton's ascites lymphoma (DLA) induced Swiss albino mice. Similarly, Chen et al. have prepared Pt nanoclusters (NCs) through the biosynthesis process by manipulating the reaction between the cancer cells such as HepG2, HeLa, or A549 cells and the platinum precursor – i.e., H_2PtCl_6 (at various concentrations) under normal culturing conditions [163]. These biosynthesized Pt NCs have exhibited in vivo fluorescence self-marking capability and also better cancer-killing efficacy via PTT when combined with porphyrin derivatives. Recently, Xie et al. have exfoliated bulk Ti in the liquid phase to form two-dimensional (2D) Ti nanosheets (NSs) to be used as a biocompatible theranostic agent as shown in Fig. 8, where these NSs have exhibited better absorption capabilities (with extinction-coefficient of 20.8 Lg^{-1} cm^{-1}) and improved photo-thermal conversion capacity (above 61%) – attributed to localized surface plasmon resonance (LSPR) phenomenon [164]. This has resulted in efficient dual-modal CT/PAI imaging-guided PTT in cervical-tumor-holding mice after NIR irradiation at 808 nm. In another similar study, Dong et al. have designed and developed renal-clearable and targeting metallic nanoparticles – FA/BSA-conjugated Bi−Bi_2S_3 heterostructured nanoparticles [165]. The following characteristics are observed for the as-prepared nanoparticles: (i) exhibited higher stability than only Bi NPs, and also possessed increased Bi-metallic content than only Bi_2S_3 NPs – resulted in improved CT imaging efficacy, (ii) shown better tumor targeting effectiveness, (iii) highly inhibited tumor cell growth after irradiating with 808 nm laser, and (iv) effective clearance after theranostics, thereby preventing unnecessary retention/toxicity.

2.4.4. *Multifunctional metallic nanoparticles*

Metallic nanoparticles (e.g., Ag, Au, Cu, and Pt) are modified as multifunctional nanoparticles by functionalizing/attaching and/or encapsulating them with other (i) contrast agents (e.g., MRI, ultrasound, and fluorophores), and (ii) therapeutic agents (for instance, magnetic hyperthermia therapy and CMT) for multimodal cancer theranostics and also drug delivery applications [166–168].

Lately, Ag-based metallic nanoparticles are changed as MNTNPs for theranostic applications. For instance, Ghaemi et al. have investigated and identified that the ZnO coatings have a major role in fine-tuning the electron-hole and flux figuration at the interface of Ag nanoparticles on UV irradiation [169]. This has consequently resulted in improved diagnostics through CT/optical imaging and also anti-tumor effects with apoptotic cell death induced in MDA-MB231 (human breast) cancer cells by activating the oxidative stress proteins. Recently, Mishra et al. have reported an easy synthesis of chitosan-coated silver-gadolinium nano-alloy (AgGd) based bimetallic nanoparticles (BNPs) with varied Ag and Gd molar ratios through the co-reduction of Ag^+ and Gd^{3+} ions, where the surface of these BNPs is loaded with DOX (via pH-sensitive hydrazone linkage) for its successful delivery for CMT cancer treatment [170]. Moreover, the presence of Gd ions has helped the BNPs to display MRI contrast with r1 & r2 values of 19.6 & 23.0 mM^{-1} s^{-1}, respectively. Besides, BNPs have emitted a CT signal intensity of 45 HU at 0.50 mg/ml concentration, which is relatively higher than the conventional CT contrast materials including iodinated complexes, barium sulfate, or metal nanoparticles. Besides, their results have demonstrated that the apoptosis of cancer cells exponentially incremented in a dose-dependent increase of DOX-loaded BNPs. In another similar

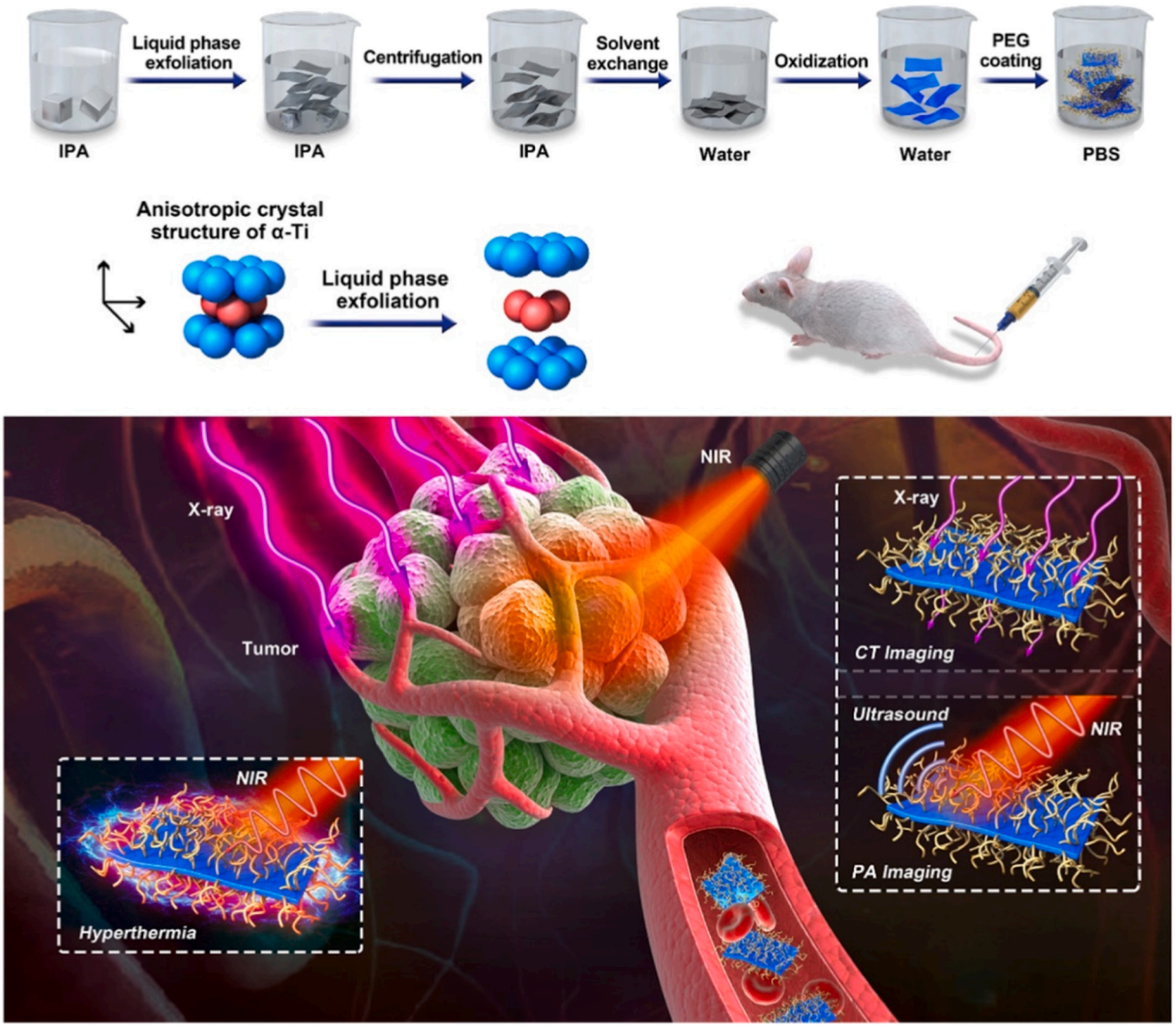

Fig. 8. Schematic representation of the exfoliation and cancer theranostic applications of TiNSs.
Reproduced with permission from Ref. [168].

investigation, the same authors have prepared chitosan-coated DOX-loaded Ag-dysprosium (Ag—Dy) BNPs, which have displayed high emission in NIR-II biological window while exciting at 808 nm [171]. Moreover, the Dy component has helped in MRI contrast studies displaying an r2 value of 7.26 mM^{-1} s^{-1}, and both Ag & Dy components revealed CT signal intensity of 46 HU. Besides, the drug carrier efficiency of BNPs is confirmed from the improved apoptotic effects (after DOX-tethering) in HeLa cancer cells. In a recent time, Sahoo et al. have prepared FA-conjugated paracetamol dimer molecules-loaded fluorescent Ag nanoclusters (AgNCs) based chitosan-composite nanoparticles, which have exhibited better theranostic efficacies in HeLa and A549 cancer cells after the differential uptake [172].

Among many recent investigations, Au-based metallic nanoparticles are specially modified as MNTNPs through different processes for use in various multimodal theranostic applications. For instance, Chen et al. have prepared glucose oxidase-conjugated plasmonic Ag/Au nanoshells (Ag/Au-GOx NSs), which have (i) proven to possess the ability for visually discriminating and screening the cancer cells in a target-free manner from the normal cells with the aid of dark-field scattering imaging and also (ii) selectively ablate the tumor cells on exposure to laser irradiation at 808 nm [173]. Similarly, Zhang et al. have made 5,10,15,20-tetrakis (4-*N*-methylpyridiniumyl)porphyrin (TMPyP4)-attached, glutathione-responsive and AS1411-aptamer conjugated mesoporous-silica-coated gold nanorods (AuNR@MS) as multifunctional nanocarriers, while using the as-formed AgNPs as the capping agents [174]. This nanocarrier has prevented the premature release of TMPyP4 and also the side-effects of the exogenous stimuli while achieving high diagnostic and therapeutic (photothermal & photodynamic) efficacies in HeLa cancer cells. Analogously, Dutta et al. have made bimetallic Au—Ag NCs and then embedded them along with a suicide gene (CD-UPRT) and a chemotherapeutic drug (5-fluorouracil (5-FC)) inside a cationic BSA nanosystem [175]. Herein, the nanosystem has created reactive oxygen species (ROS) through Au—Ag NCs and apoptosis via suicide gene along with 5-FC during the combined therapy of HeLa cancer cells, while luminescence-based bioimaging was performed with the aid of NCs. Recently, Zhou et al. have reported the preparation and consequent characterization of PEI-entrapped FA-targeted Au nanoparticles (chelated with Gd ions) to form a nanoparticulate system [176]. This system has displayed superior X-ray attenuation properties and also sensible r1 relaxivity of 1.1 mM^{-1} s^{-1}, which have made FA-targeted Au nanoparticles an effectual nanoprobe for dual-mode tumor imaging (CT & MRI). Similar investigations are performed by the same authors for dual-mode tumor imaging [177,178]. Analogously, Wang et al. have initially conjugated cyptate (Cy - indocyanine green-based a NIR fluorophore) on the surface of hollow Au nanospheres via a short spacer – i.e., urokinase-type plasminogen activator (uPA - a breast cancer enzyme) enzyme-substrate-motif (G-G-R) [179]. The conjugated Au nanospheres have helped in specific

fluorescence visualization and consequent hyperthermia killing of tumor cells. In another study, Mangadlao et al. have made prostate-specific membrane antigen (PSMA-1)-targeted PEG-coated Au nanoparticles that are functionalized with Pc4 molecules and loaded with anti-cancer drugs [180]. Herein, the nanoparticles are highly up-taken (up to 4 folds) by PSMA-positive PC3pip cells as compared to PSMA-negative PC3flu cells, which have resulted in enhanced targeted theranostics (via fluorescence-imaging-guided PDT) under in vivo environment. Recently, Dong et al. have designed and made anti-human epidermal growth factor receptor 2 (HER2) antibodies-functionalized Au-nanoshelled poly(lactic-*co*-glycolic acid) based magnetic hybrid nanoparticles, which have exhibited contrast-enhanced ultrasound (US) imaging and MRI (r2 = 441.47 mM^{-1} s^{-1}) [181]. Herein, HER2 functionalization on nanoparticles has significantly improved their US/MRI imaging effects in targeted cells, and explicitly induced SKBR3 cell death on exposure to NIR laser irradiation via PTT. In a similar investigation, Zhao et al. have formed ^{131}I—Au PENPs-CTX nanocomplex by sequentially functionalizing PEI template with different molecules (such as PEG, glioma-specific peptide (i.e., chlorotoxin, CTX) and 3-(4-hydroxyphenyl) propionic acid-OSu) and also entrapped iodine-radiolabeled (^{131}I) Au nanoparticles [182]. The as-formed complex has successfully been tested for targeted (single-photon emission computed tomography) SPECT/CT imaging, and also radio-nuclide therapy of glioma cancer cells. In another study, Emami et al. have initially conjugated DOX and anti-PD-L1 antibodies (to target PD-L1 (B7-H1/CD274) - type I transmembrane protein, overexpressed in colorectal cancer (CT-26) cells) to the α-terminal end groups of lipoic acid-PEG-N-hydroxysuccinimide (LA-PEG-NHS), which is then attached to the surface of Au nanoparticles to form PD-L1-AuNP-DOX nanocomplexes [183]. The antibodies have increased the intracellular uptake of nanocomplexes and also their retention, which has subsequently improved their therapeutic efficacy by synergistically inhibiting CT-26 cancer cell growth via chemo-photothermal therapy (through DOX exposure and NIR irradiation).

Similarly, Cu, Pt, and other metallic nanoparticles are also modified as MNTNPs for cancer treatments. For example, Pang et al. have explicitly introduced radioactive ^{64}Cu atoms into the crystal lattice of palladium, which is then covered with Au, to form core-shell nano-tripods as shown in Fig. 9 [184]. Herein, the Au shell has been formed to prevent the oxidation and dissolution of Cu/^{64}Cu atoms and also to provide strong absorption at the NIR region for PTT. Moreover, the core-shell structure is conjugated with D-Ala1-peptide T-amide (DAPTA) to improve the targeting of C − C chemokine receptor 5 (CCR5) towards TNBC cells. Furthermore, the as-prepared tripod nanostructures have displayed enhanced PTT efficacy in TNBC-induced-orthotropic-mouse (4 T1 mouse) models via PET-image-guidance. Analogously, Patel et al. have focused their investigation on improving the Pt-based cancer therapy by forming a nanoemulsion formulation (NMI-350, 351 or 352) by co-encapsulating di-fatty acid platins (i.e., dimyristplatin, dipalmiplatin, or distearyplatin respectively) and C6-ceramide in its lipid core and lipidated gadolinium & FA (for imaging & targeting) on its surface [185]. Among all, NMI-350 based nanoformulation is highly competent in MRI imaging, and cisplatin-resistant KBCR-1000 cancer therapeutics.

2.5. Magnetic nanoparticles

2.5.1. Superparamagnetic Iron oxide nanoparticles (SPIONs)

Superparamagnetism is a unique behavior of magnetic nanoparticles to exhibit magnetic saturation under an applied magnetic field, while not showing any residual magnetism after the removal of the magnetic field [186]. Superparamagnetic iron oxide nanoparticles (SPIONs) are single-domain particles with a typical size of less than 15–20 nm with the capability to reveal high saturation magnetization (Ms) and high initial susceptibility in presence of an external magnetic field while able to completely demagnetize by removal of the magnetic field with negligible (nearly zero) coercivity and magnetic remanence (Hc ≈ Mr. ≈ 0) at room temperature. In a biomedical application, SPIONs are commonly used in the form of ferrofluids which are nothing but a homogeneous stable colloidal suspension of SPIONs dispersed in a carrier fluid, usually water. Over the past few years, SPIONs are extensively used as very effective MNTNPs due to their ability (i) to carry anticancer drugs to the tumor site (drug delivery via magnetic targeting), (ii) to enhance MRI contrast for better tumor imaging, and (iii) to induce magnetic hyperthermia and ROS based therapy as a substitute for CMT or RT in cancer treatment [187]. The theranostic efficacy strongly relies upon generating narrow size distribution and well-dispersed SPIONs in an aqueous ferrofluid suspension. However, uncoated SPION tends to agglomerate in water or tissue fluid, which may limit many clinical applications. Hence, SPIONs are commonly stabilized in an aqueous ferrofluid suspension by two approaches: electrostatic (ionic)

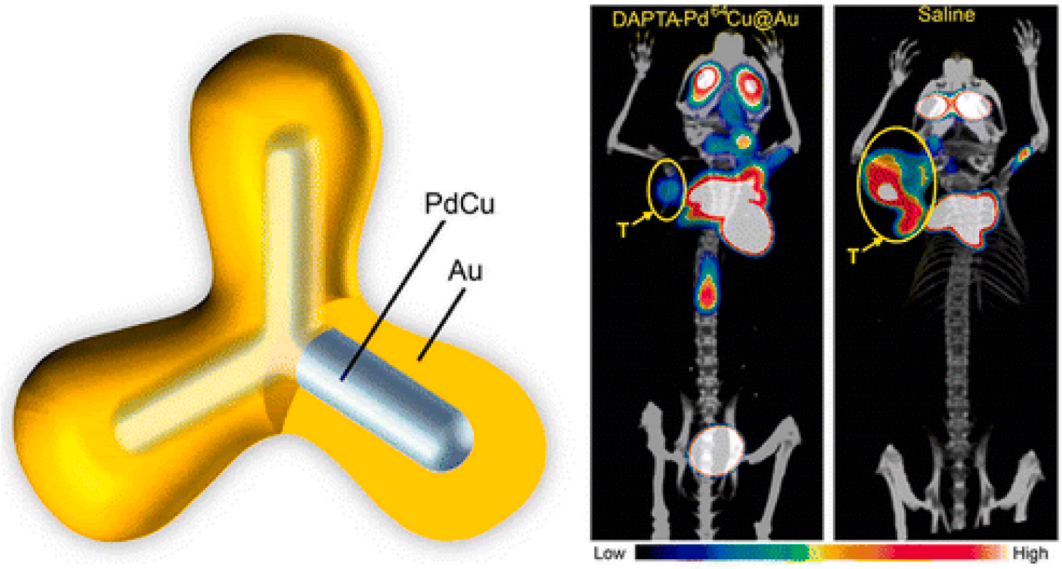

Fig. 9. Schematic of the PdCu–Au core-shell based tripods tripod (which can be prepared by coating the surface of a PdCu tripod with a conformal shell made of Au) and their utilization in PET/CT imaging of mice injected with tripod.
Reproduced with permission from Ref. [188].

interactions of surface charges; (ii) steric repulsions of a hydrophilic surface coating such as surfactant (e.g. fatty acids) molecules, gold/silica, or polymeric (e.g. dextran, polyvinyl alcohol) shell. Apart from physical and biological synthesis, SPIONs can be effectively prepared by various chemical methods such as co-precipitation, thermal decomposition, microemulsion, hydrothermal, sonochemical, microwave-assisted synthesis methods [188]. However, co-precipitation and thermal decomposition are mostly preferred to synthesize SPIONs with narrow size distribution due to their simplicity, reproducibility, scalability, versatility (possibility of size/morphology control with tunable functionality), purity, rapidness, and cost-effectiveness [189–191]. For example, Maity et al. have reported co-precipitation/thermolysis synthesis of high quality (i.e. controlled size, phase pure, controlled sized/shaped, and highly water dispersed) SPIONs and clusters with improved magnetization, biocompatibility, T2 relaxivity, and SAR for enhanced MRI and efficient MFH [192,193].

Further, SPIONs are increasingly modified/functionalized and/or co-encapsulated with anticancer drugs within various biocompatible/biodegradable polymer such as PLGA, poly-ε-caprolactone (PCL), chitosan (CHI), PEG, etc. by simple oil-in-water emulsion/solvent evaporation or nanoprecipitation method to develop magnetic polymeric nanosystems for controlled/triggered drug release while performing simultaneous cancer imaging and treatment [194–198]. For instance, Huanrong et al. have developed folate receptor-targeted, pH-sensitive, and DOX loaded magnetic-polymeric nanocarriers based on poly (β-aminoester) functionalized SPIONs for cancer treatment and imaging [199]. These magnetic polymeric-based smart DDS are capable of carrying the desired amount of drug to deliver/release at the target in a controlled and sustained manner.

Polymeric encapsulation is very crucial to impart a series of benefits to the SPIONs such as chemical stability (by protecting particle surfaces from oxidation), multi-loading capacity (co-encapsulation of drugs with other therapeutic/imaging agents), dispersibility with narrow size distribution (colloidal stability by preventing agglomeration), reduction of toxicity (biocompatibility with organic ingredients) and functionality (for binding drugs by covalent attachment, adsorption or entrapment on the particles). In particular, SPIONs based ferrofluids have been extensively focused on cancer theranostics to use them as targeted drug delivery systems, MRI contrast agents, and therapeutic agents in magnetic hyperthermia. However, the effectiveness of the SPIONs (ferrofluids) depends on their physicochemical/magnetic/thermal/pharmacological properties that include chemical composition, morphology, crystal structure, granulometric uniformity, magnetization, surface-structure, adsorption properties, dispersibility, stability, and biocompatibility (toxicity). These properties are considerably impacted by the synthesis methods and surface-stabilization processes.

2.5.1.1. Magnetic resonance imaging (MRI). SPIONs produce negative (dark) contrast based on T2-weighted images by shortening the transverse spin-spin relaxation (T2 i.e. inverse of r2 relaxivity, 1/r2) while paramagnetic complexes (including gadolinium (Gd^{3+}) or manganese (Mn^{2+}) ions) produce positive (bright) contrast based on T1-weighted images by shortening the longitudinal spin-lattice relaxation (T1 i.e. the inverse of r1 relaxivity, 1/r1) depending on the magnetic interactions with nearby water protons surrounding the tissue [200,201]. However, SPIONs have been widely used as commercial MRI T2 contrast agents (to generate dark negative contrast) for cancer detection/imaging due to their following advantages: (i) biocompatibility (readily sequestered and metabolized by the body); (ii) higher MRI signal contrast/sensitivity (strong *T*2 shortening effect); (iii) biodegradability (able to decompose into Fe^{2+}/Fe^{3+} and mix with blood); and (iv) quick detectability (via TEM) over the paramagnetic (Gd(III)/Mn(II)) complexes [202–205]. The contrast property of the SPIONs is mainly influenced by their saturation magnetization value depending on their particle size, shape, composition, crystal structure, and surface coatings. Jun et al. have demonstrated that MRI contrast increases with the increase in the size of the SPIONs because larger SPIONs have a higher magnetization than the smaller counterparts [206]. Similarly, Maity et al. have reported very high MRI r2 values of 735.3/450.8 mM^{-1} s^{-1} for terephthalic acid (TA)/2-aminoterephthalic acid (ATA)-coated SPIONs respectively, due to high crystallinity and/or effective spin transfer through π–π conjugation of surface-attached TA/ATA molecules which probably manifested better magnetic response to the magnetic field [207]. In other studies also, better r2 relaxivity values are reported - Karagoz et al. (550 mM^{-1} s^{-1} at 9.4 T) for POEGMA-b-PMAA-b-PST-triblock-copolymer-encapsulated-SPIONs, and Lin et al. (514.7 and 596.8 mM^{-1} s^{-1} at 1.5 T) for PEI-(with 2 different formulations)-coated-SPIONs [208]. Besides MRI, magnetic particle imaging (MPI) has been emerged as a very promising non-invasive 3D imaging technique based on the SPIONs tracers due to its advantages like high sensitivity/contrast, zero ionizing radiation. For instance, Tay et al. have demonstrated SPIONs as MNTNPs for MPI image-guided MHT cancer treatment [209].

2.5.1.2. Magnetic hyperthermia therapy (MHT). Magnetic hyperthermia therapy (MHT, also known as MFH) is a highly localized cancer therapeutic approach to inhibit tumor cell growth/viability at elevated temperatures (above 41 °C) or to produce a heat-induced cytotoxic effect with minimal side effects than other alternative cancer treatment modalities such as CMT or RT. In MHT, SPIONs are delivered (intravenously injected and accumulated) at the tumor site, and then the temperature of the tumor cells locally raised to the therapeutic temperature (42–46 °C) on exposure to an external alternating magnetic field (AMF) with a radiofrequency. The heating efficiencies of the SPIONs can be measured by calorimetric MFH experiments (as shown in Fig. 10) which can be performed under variable AMF (amplitude /frequency) conditions. The heating efficiencies are generally expressed in terms of specific absorption rate (SAR in W/g) and intrinsic loss power (ILP in nHm^2 kg^{-1}) using the following equations.

$$SAR = \frac{m_{samp} c_{samp}}{m_{Fe}} \frac{\Delta T}{\Delta t}$$

$$ILP = \frac{SAR}{H^2 f}$$

where m_{samp} is the total mass of the ferrofluid sample (in g) taken for the measurement, c_{samp} is its specific heat capacity (in $J.kg^{-1}.K^{-1}$), m_{Fe} is the mass of the magnetic element in the sample (Fe in g), $\Delta T/\Delta t$ is the initial slope of time-dependent temperature curve, H is the applied magnetic field amplitude and f is the frequency of the magnetic field.

The SAR value depends on the properties of the SPIONs such as their size/shape, crystal structure, magnetization, and dispersity in aqueous media. It is detected that polydispersity (containing particles of different sizes) samples can give rise to inferior SAR/ILP values. Recently, Kandasamy et al. have reported different small chain surfactants molecules (e.g. polyol, carboxyl amine benzene) coated SPIONs (~5–15 nm) and SPIONs clusters with high magnetization and narrow size distribution to exhibit very high SAR values (~450–900 W/g) at a field amplitude of 24.5 KA/m and a frequency of 400 kHz) [210–214]. Similarly, Prashant et al. have reported improved SAR values for PLGA/Pluronic polymers encapsulated SPIONs, where the encapsulation has been very helpful in overcoming the RES uptake [215,216]. Recently Salunkhe et al. have demonstrated next-generation MRI-guided magneto-CMT with ~96% killing efficiency of breast cancer (MCF7) cells by using Pluronic F127 micelle-encapsulated diisopropylamine-stabilized SPIONs (having size ~12 nm, magnetization of 92 emu g^{-1} and SAR ~717 wg^{-1}) based ferrofluids at 1 mg/ml concentration on exposure to AMF (20 kAm^{-1}, 267 kHz) for 30 min [217]. Recently, Kandasamy et al. have co-encapsulated SPIONs with dual drugs (curcumin with verapamil/nifedipine (a calcium channel blocker to prevent MDR)) inside

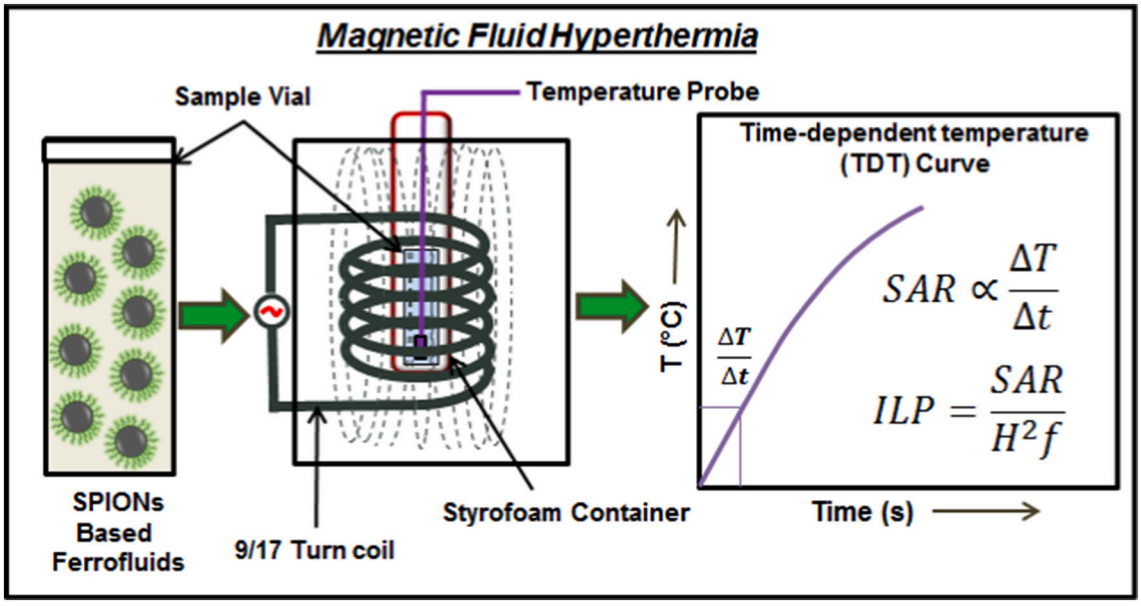

Fig. 10. Schematic of calorimetric magnetic fluid hyperthermia studies.

biocompatible polymers, which subsequently have showed enhanced therapeutic efficacy in CMT/MHT based HepG2 cancer treatments [197,198].

2.5.2. *Multifunctional SPIONs*

SPIONs are surface-modified not only to reduce their agglomeration or protect their surfaces from oxidation but also to implant surface functional groups (anchor points) to chemically link with therapeutic molecules/agents such as drugs, fluorescent molecules, C_{60}, gold, photosensitizer, and so on [218–220]. These therapeutic molecules/agents can be immobilized (bound) with SPIONs either by co-encapsulation in nanocarriers or by grafting (attachment) on the surface of SPIONs [221–223]. Surface functionalized SPIONs have emerged as potential smart nanocarriers/DDS and also MNTNPs for use in MRI/FI/PAI guided cancer therapeutic applications (CMT, RT, and MHT) [224–226]. Moreover, SPIONs are conjugated with various targeting ligands such as antibodies, small molecular ligands, aptamers through bio-conjugation (either directly or by molecular cross-linkers) for accomplishing targeted drug delivery to improve their selective tumor accumulation, while increasing their blood circulation by preventing the RES uptake, and reducing non-specific targeting [227–229]. Furthermore, SPIONs are associated with stimuli-responsive polymers via electrostatic/hydrophobic interactions or encapsulated in the biocompatible coating to achieve controlled/triggered release at the target tumor site in response to the environmental change such and pH, temperature, light, enzymatic, magnetic field change, while enhancing the drug specificity and potency of effective cancer treatment with reduced side effects [230–232]. Indeed, there is a very vital necessity to functionalize the SPIONs with both the targeting ligands and stimuli-responsive agents to improve their accumulation and controlled/triggered release at the target tumor site and thereby to enhance the T2 contrast and localized heating for effective tumor growth inhibition to achieve imaging-guided cancer treatment beside delivering other therapeutic and imaging agents for accomplishing multimodal theranostics. For example, Kaaki et al. have prepared FA-conjugated DOX-loaded PEG-coated SPIONs as MNTNPs [233]. These MNTNPs have exhibited excellent biocompatibility, significant cell uptake by MCF-7 cancer cells, and bimodal cancer cell imaging via MRI/FI, besides showing efficient targeting and MHT effects. Similarly, Kievit et al. have reported that fluorescent dye-labeled and PEGylated SPIONs are conjugated with mouse IgG for metastatic breast cancer targeted delivery, therapy, and imaging [234]. Later, Hayashi et al. have conjugated FA with PEG-modified SPIONs based nanoclusters (with high relaxivity and SAR values) to enhance their targeted accumulation in a mice tumor (after 24 h of iv), while escaping from their penetration in normal tissues for improved localized heating and MRI contrast of the tumor [235]. Similarly, Beeran et al. have made SPIONs embedded hydroxyapatite (HAIO) nanoparticles, which have exhibited 75% cancer cell death via MHT and high T2 relaxivity of 50.92 mM^{-1} s^{-1} in MRI [236].

El-Dakdouki et al. have reported hyaluronan-coated and DOX-conjugated SPIONs (DOX-HA-SPION) as a promising magnetic DDS for cancer imaging and treatment due to their excellent biocompatibility, rapid cancer cell internalization, and killing ability of multi-drug-resistant/sensitive ovarian cancer cells [237,238]. The DOX-HA-SPIONs have exhibited improved MRI and significant reduction of tumor growth which have led to the longer survival of the tumor-induced mice. Similarly, SPIONs-encapsulated HA based polymeric micelles are reported as very promising theranostic nanoplatforms for enhanced accumulation in intramuscular tumor, improved MRI, and significant growth inhibition of colon adenocarcinoma (HT-29) cells via ROS formation [239]. These micelles (having the size of ~100 nm) have demonstrated high SPIONs loading capacity, greater intracellular uptake/release, high T2 relaxivity, and selective cytotoxicity to the tumor in vivo. Similarly, Wu et al. have conjugated α-ketoglutarate-modified SPIONs with lymphatic vessel endothelial hyaluronan receptor 1 and Podoplanin for dual-targeting to mark the lymphatic endothelial cells in metastatic tumors [240]. Analogously, Huang et al. have reported pH-responsive SPION-micelles that are loaded with an anticancer drug β-lapachone (β-lap) as theranostic nanomedicines to improve the therapeutic efficacy by selective release via the micelles and increasing (10-fold) ROS stress for achieving significant cancer cell death, besides doing MRI imaging [241]. Likewise, Chiang et al. have made DOX-loaded hollow inorganic/organic hybrid nanogels as multimodal theranostic nanoplatforms for pH/temperature-stimulated MRI imaging and MHT/CMT by grafting the citric acid-coated SPIONs with copolymer consisting of acrylic acid/2-methacryloylethyl acrylate and PEG/poly(N-isopropylacrylamide) [242]. These nanoplatforms have shown enhanced stimuli-triggered drug release and synergetic combination of hyperthermia and MRI.

Recently, Lee et al. have reported non-polymeric biocompatible adenosine triphosphate (ATP - an innate biomaterial derived from the body)-coated SPIONs (as an advanced contrast agent), whose surface is

modified with gluconic acid and conjugated with cMet-binding peptide and Cy5.5 and labeled with ^{125}I for efficient multimodal imaging (refer Fig. 11) of U87MG cancer cells and tumor in mice models via MRI and SPECT/CT imaging [243]. The as-prepared SPIONs have also exhibited rapid degradation (as compared to ferumoxides), reduced phagocytic uptake, improved biodistribution, and effective tumor targeting in vivo. Similarly, Carrouee et al. have developed MNTNPs by combining Ag NPs and VNIR dye Nile Blue (NB) with SPIONs for multimodal imaging based on MRI, surface-enhanced resonant Raman scattering (SERRS), and NIR-FI [244]. Likewise, Chen et al. have conjugated bovine serum albumin (BSA)-gadolinium complexes with MoS_2 nanoflakes as MNTNPs for bi-modal MRI/PAI and PTT of xenograft tumors [245]. The as-synthesized MoS_2 – Gd – BSA have exhibited high biocompatibility, photostability and combined MRI/PAI guided photothermal effects for effective cancer theranostics. Manigandan et al. have developed PEGylated micelles that are anti-αvβ3 integrin antibody conjugated and DOX/SPIONs loaded [246]. These micelles have shown improved internalization into drug-resistant MDA-MB-231 and enhanced theranostic efficacy via simultaneous MRI and MHT.

Similarly, Wang et al. have prepared MNTNPs, by conjugating fibronectin-targeted and endogenous enzyme-activated SPIONs with Cys-Arg-Glu-Lys-Ala (CREKA) peptide and squaraine photosensitizer for boosted MRI-guided FI and PDT of triple-negative breast cancer (TNBC) tumors [247]. They have demonstrated an increased capability for the as-prepared MNTNPs in real-time monitoring of the size reduction of MDA-MB-231 and MCF-7 tumors (via FI) in mice models due to enhanced PDT effects (as shown in Fig. 12). Tiwari et al. have reported FA- conjugated and 5-flouoruracil functionalized SPIONs based targeted nanosystems for bi-modal MRI/fluorescence imaging [248]. These magneto-fluorescent nanoparticles have demonstrated strong fluorescence emission, excellent biocompatibility, good stability, enhanced pH-stimulated drug release (92%), and improved T2-weighted MRI (T2-MRI) contrast for efficient cancer imaging. Similarly, Vijayan et al. have developed photo-luminescent SPION based theranostic nanogels, which have exhibited enhanced dual FI/MRI-guided MHT [249]. Likewise, Das et al. have embedded CDs onto the surface of the SPIONs for bimodal T2-MRI/FI in cancer treatments applications [250]. Recently, Pan Animesh et al. have co-loaded DOX and SPIONs into the core of liposomes, which are then conjugated with thiol-terminated PEG-modified gold nanoparticles for use in radio-frequency (RF)/NIR-stimulated and triggered drug release for aiding CMT in combination with MHT [251]. The magneto-liposomes have exhibited high cellular uptake and enhanced therapeutic effects on A549 (human lung cancer) cells. Similarly, Tiwari et al. have developed graphite carbon-coated SPIONs based magneto-

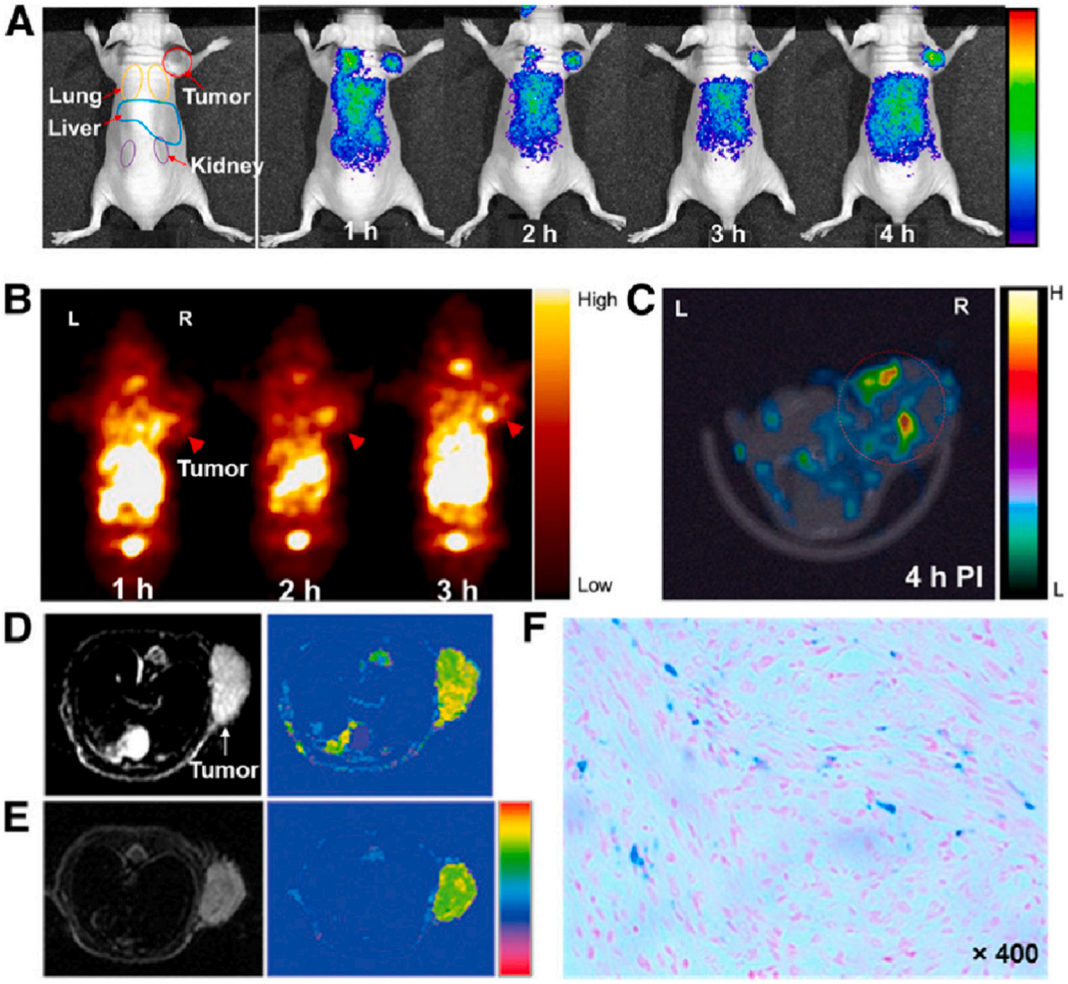

Fig. 11. Multimodality tumor imaging using cMBP-GA-ATP@SPIONs. (A) In vivo noninvasive near-infrared fluorescent images of mice with U87MG tumors. Images were taken at 1, 2, 3, and 4 h after injection of CMG-ATP@SPIONs. (B) In vivo static planar g images of mice with U87MG tumors. Images were taken at 1, 2, and 3 h after injection of 125I-cMBP-GA-ATP@SPIONs. (C) Reconstructed coregistered transverse SPECT/CT image of same mouse 4 h after injection. In vivo T2-weighted MR images of mice with U87MG tumors were obtained before (D) and at 3 h after (E) injection of cMBP-GA-ATP@SPIONs. (F) Prussian blue staining on tumor sections. Blue dots, representing iron contents, were widely found across tumor, with inhomogeneous pattern. PI 5 after injection. (For interpretation of the references to colour in this figure legend, the reader is referred to the web version of this article.)
Adapted from Ref. [247].

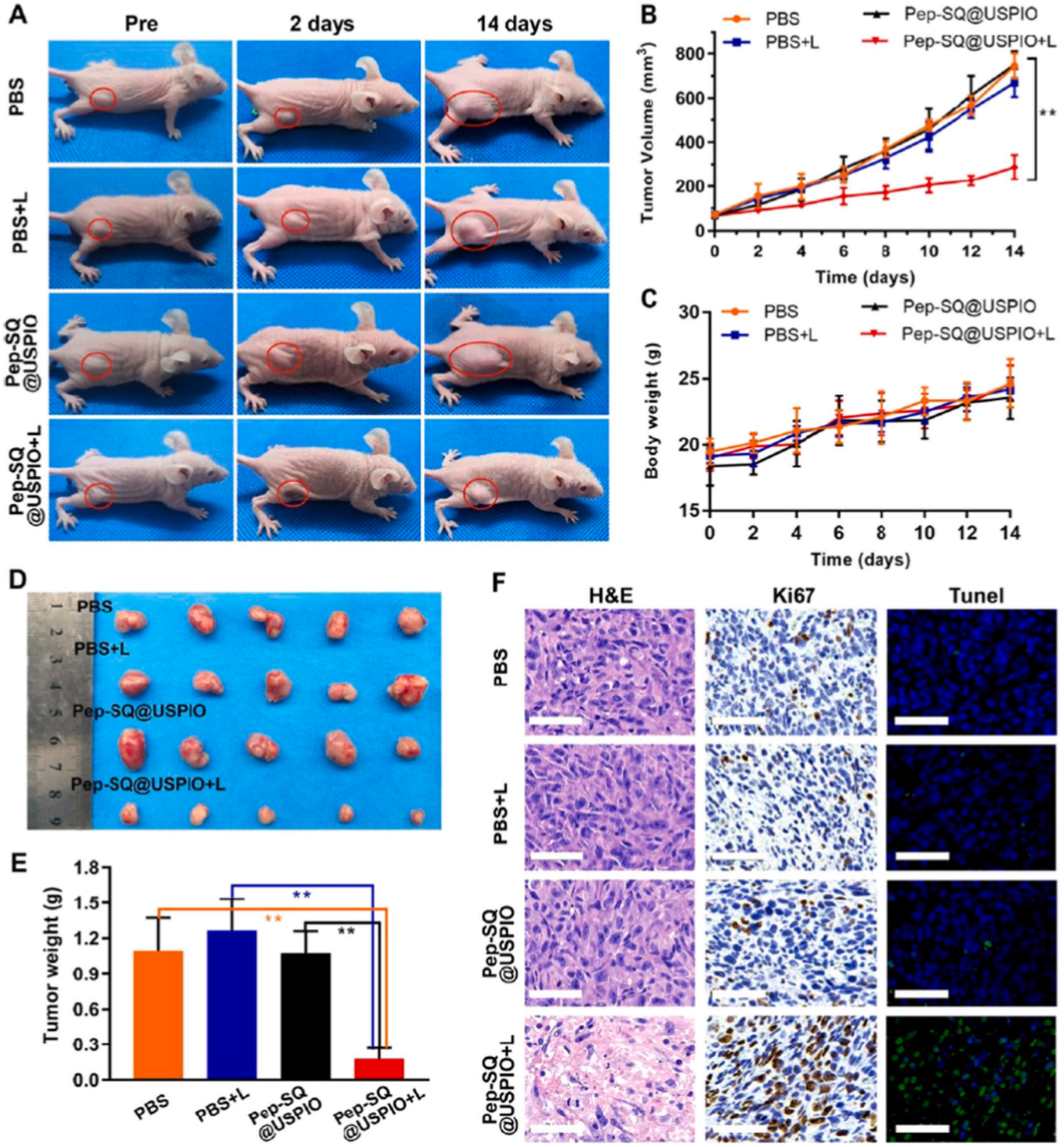

Fig. 12. In vivo PDT of TNBC. (A) Photographs of MDA-MB-231 tumor-bearing mice during PDT. (B) Tumor volume curves and (C) weight growth curves of mice over time in each group, including PBS, PBS + L, Pep-SQ@USPIO, and Pep-SQ@USPIO + L. L indicates NIR laser (660 nm, 2 W/cm2). (D) Images and (E) weights of exfoliated tumors of each group after treatments. (F) Histochemical analysis (H&E, Ki67, Tunel) of tumor sections in each group. Scale bar: 50 μm. Adapted from Ref. [251].

fluorescent nanoprobes which showed promising cancer theranostic effects via bi-modal MRI/FI guided MHT [252].

2.5.3. *Other functionalized magnetic nanoparticles*

Fan et al. have developed Cy3 surface-functionalized and S6 aptamer conjugated magnetic iron-plasmonic gold core-shell based and star-shaped MNTNPs for targeted imaging, separation, and photothermal ablation of tumors [253]. These MNTNPs have displayed excellent NIR-FI and selective PTT effects for irreversible damage of the SK-BR-3 cancer cells. Likewise, Zhang et al., have reported BSA-conjugated manganese-doped iron oxide (MnIO) based MNTNPs for T1-weighted MRI-guided PTT of the tumors [254]. Moreover, Sancey et al. have reported gadolinium-based nanoparticles as biocompatible MNTNPs for potential MRI contrast agents and radio-sensitizers for X-ray cancer

treatment [255]. Lately, Thorat et al. have developed DOX and superparamagnetic $La_{0.7}Sr_{0.3}MnO_3$ loaded oleic acid-PEG micelles for MHT applications [256]. These micelles have exhibited high drug loading capacity (~60.45%), drug releasing capability, biocompatibility, and improved cancer cell killing efficiency (89%) via MHT-CMT. Besides, Kim et al. have designed biocompatible $MnFe_2O_4$-functionalized MSNs to overcome hypoxia to improve therapeutic efficiency of PDT by exploiting continuous O_2-evolving property of $MnFe_2O_4$ nanoparticles through the Fenton reaction [257]. The as-prepared MSNs have revealed enhanced MRI-guided PDT effects in in vivo cancer theranostics. Likewise, Yang et al. have made SPIONs-embedded WS nanocomposites as MNTNPs that are functionalized with PEG-modified MSNs and further loaded with DOX for multimodal FI, MRI and X-ray computed tomography (CT) imaging-guided synergetic PTT and CMT [226]. The as-prepared MNTNPs displayed triggered release, strong NIR light, and X-ray absorbance, and effective cancer cell killing through NIR-irradiated photothermal heating and chemotherapeutic effect. Later, Patra et al. have reported Fe^{3+}-terpyridine nanocomplex that are functionalized with PEG-FA and DOX for efficient T1 weighted MRI, pH-responsive delivery, and effective treatment of prostate cancers [258]. Likewise, Chu et al. have developed copper sulphide (CuS)@BSA core-shell based MNTNPs for simultaneous MRI and PTT [259]. The as-prepared nanoparticles have exhibited excellent biocompatibility, strong NIR absorption, high T1-weighted MRI contrast (compared to clinically used Magnevist), and effective photothermal ablation of cancer cells. Similarly, Wang et al. have reported PEG-modified MNTNPs loaded with IR820 and Fe^{3+} ions for use in bimodal imaging and therapy [260]. The as-prepared MNTNPs have exhibited good biocompatibility, improved cell uptake, combined PAI/MRI, and also capability of generating significant heat and ROS for achieving synergetic PTT/PDT effects for efficient cancer detection and treatment. As similar to SPIONs, Mn − Zn ferrite NPs are emerged as TNPs due to their significant potential for getting applied in simultaneous MRI, DDS, and MHT in cancer theranostics. Sun et al. have prepared worm-like PEG/RGD-modified $Mn_{0.63}Zn_{0.37}Fe_2O_4$ nanoparticles and then conjugated them with PTX [261]. These MNTNPs have exhibited targeted delivery, controlled drug release, improved bimodal T2-MRI/FI, and higher killing of tumor cells for effective cancer theranostics.

3. Conclusions and perspectives

In this review, we have reviewed the recently-developed multifunctional TNPs – i.e., mesoporous silica nanoparticles, luminescence nanoparticles, carbon-based nanomaterials, metal nanoparticles, and magnetic nanoparticles – and their use in state-of-the-art cancer biomedical applications such as drug delivery, diagnostics/imaging (i.e., MRI, PET, SPECT, PAI), and therapeutics (i.e., CMT, PTT, PDT, MHT) efficiently and simultaneously. It has been noted from different investigations that the functionalized TNPs (as compared to non-functionalized counterparts) have emerged as potential and smart nanomedicines by ensuring better bioavailability, tumor-specific targeting, controlled/triggered (stimuli-responsive) release, and efficient cancer theranostic action. Moreover, the functionalization has helped in reducing various limitations available in the conventional CMT.

Though a variety of multifunctional TNPs are being developed and applied for cancer treatments throughout the world, a complete alternative to CMT or any other conventional cancer treatments has not been attained so far. This is mainly due to the barriers like toxicity, biodistribution and so on that are associated with the as-developed multifunctional TNPs. Moreover, there is still a lack of continuous research studies that investigate the complete effectiveness of these TNPs in different cancer environments –from in vivo to clinical trials. Because of this, the clinical translation of cancer treatments via multifunctional TNPs is still questionable. However, research work on the TNPs is continuously moving forward at a fast pace to overcome the above-mentioned challenges to be successfully applied as effective nanomedicines for early cancer diagnosis and image-guided treatments besides providing an alternative solution to the existing treatment modalities.

Declaration of competing interest

Authors report no conflicts of interest in this work.

Acknowledgments

We would like to acknowledge the previously reported works by the researchers who have been cited in this review paper.

References

[1] R.L. Siegel, K.D. Miller, A. Jemal, CA Cancer J. Clin. 65 (2015) 5–29.
[2] E. Robinson, J. Mohilever, J. Zidan, D. Sapir, Cancer 54 (1984) 1454–1460.
[3] P. Autier, M. Boniol, Eur. J. Cancer 90 (2018) 34–62.
[4] D. Ilic, M. Djulbegovic, J.H. Jung, E.C. Hwang, Q. Zhou, A. Cleves, T. Agoritsas, P. Dahm, BMJ 362 (2018) k3519.
[5] S.S. Ahmad, M.A. Reinius, H.M. Hatcher, T.V. Ajithkumar, BMJ 17 (2016) i4567.
[6] S.S. Ahmad, M.A. Reinius, H.M. Hatcher, T.V. Ajithkumar, BMJ 354 (2016) i4567.
[7] K.O. Alfarouk, C.-M. Stock, S. Taylor, M. Walsh, A.K. Muddathir, D. Verduzco, A. H.H. Bashir, O.Y. Mohammed, G.O. Elhassan, S. Harguindey, S.J. Reshkin, M. E. Ibrahim, C. Rauch, Cancer Cell Int. 15 (2015) 71.
[8] X. Wang, L. Yang, Z. Chen, D.M. Shin, CA Cancer J. Clin. 58 (2008) 97–110.
[9] A.S. Thakor, S.S. Gambhir, CA Cancer J. Clin. 63 (2013) 395–418.
[10] L. Dai, J. Liu, Z. Luo, M. Li, K. Cai, J. Mater. Chem. B 4 (2016) 6758–6772.
[11] Y.H. Bae, K. Park, J. Control. Release 153 (2011) 198–205.
[12] C. Ding, L. Tong, J. Feng and J. Fu, Molecules, 2016, 21, 1715.
[13] C. Han, H. Huang, Y. Dong, X. Sui, B. Jian, W. Zhu, Molecules 24 (2019) 1–14.
[14] H.-J. Liu, P. Xu, Nanomaterials 9 (2019) 511.
[15] M. Gisbert-Garzarán, M. Manzano and M. Vallet-Regí, Pharmaceutics, DOI: https://doi.org/10.3390/pharmaceutics12010083.
[16] Z.-A. Qiao, B. Guo, A.J. Binder, J. Chen, G.M. Veith, S. Dai, Nano Lett. 13 (2013) 207–212.
[17] Y. Chen, H.R. Chen, J.L. Shi, Acc. Chem. Res. 47 (2014) 125–137.
[18] E. Yamamoto, M. Kitahara, T. Tsumura, K. Kuroda, Chem. Mater. 26 (2014) 2927–2933.
[19] S. Wang, M. Chen, L. Wu, ACS Appl. Mater. Interfaces 8 (2016) 33316–33325.
[20] N.T. Vo, A.K. Patra, D. Kim, Langmuir 34 (2018) 3901–3908.
[21] P. Yan, X. Zhang, X. Wang, X. Zhang, Langmuir 36 (2020) 5271–5279.
[22] A.F. Moreira, D.R. Dias, I.J. Correia, Microporous Mesoporous Mater. 236 (2016) 141–157.
[23] R. Chakravarty, S. Goel, H. Hong, F. Chen, H.F. Valdovinos, R. Hernandez, T. E. Barnhart, W. Cai, Nanomedicine 10 (2015) 1233–1246.
[24] M.K. Gurka, D. Pender, P. Chuong, B.L. Fouts, A. Sobelov, M.W. McNally, M. Mezera, S.Y. Woo, L.R. McNally, J. Control. Release 231 (2016) 60–67.
[25] A. Tukappa, A. Ultimo, C. De La Torre, T. Pardo, F. Sancenón, R. Martínez-Máñez, Langmuir 32 (2016) 8507–8515.
[26] Y.J. Cheng, G.F. Luo, J.Y. Zhu, X.D. Xu, X. Zeng, D.B. Cheng, Y.M. Li, Y. Wu, X. Z. Zhang, R.X. Zhuo, F. He, ACS Appl. Mater. Interfaces 7 (2015) 9078–9087.
[27] Y. Zhang, C.Y. Ang, M. Li, S.Y. Tan, Q. Qu, Z. Luo, Y. Zhao, ACS Appl. Mater. Interfaces 7 (2015) 18179–18187.
[28] J. Poostforooshan, S. Belbekhouche, M. Shaban, V. Alphonse, D. Habert, N. Bousserrhine, J. Courty, A.P. Weber, ACS Appl. Mater. Interfaces 12 (2020) 6885–6898.
[29] F. Chen, H. Hong, Y. Zhang, H.F. Valdovinos, S. Shi, G.S. Kwon, C.P. Theuer, T. E. Barnhart, W. Cai, ACS Nano 7 (2013) 9027–9039.
[30] C. Argyo, V. Weiss, C. Bräuchle, T. Bein, Chem. Mater. 26 (2014) 435–451.
[31] M. Martínez-Carmona, M. Colilla, M. Vallet-Regí, Nanomaterials 5 (2015) 1906–1937.
[32] W. Chen, C.A. Cheng, J.I. Zink, ACS Nano 13 (2019) 1292–1308.
[33] L. Dai, Q. Zhang, J. Li, X. Shen, C. Mu, K. Cai, ACS Appl. Mater. Interfaces 7 (2015) 7357–7372.
[34] R.K. Singh, T.H. Kim, C. Mahapatra, K.D. Patel, H.W. Kim, Langmuir 31 (2015) 11344–11352.
[35] T. Nakamura, F. Sugihara, H. Matsushita, Y. Yoshioka, S. Mizukami, K. Kikuchi, Chem. Sci. 6 (2015) 1986–1990.
[36] C. Hu, P. Huang, Z. Zheng, Z. Yang, X. Wang, Langmuir 33 (2017) 5511–5518.
[37] L. Chen, X. Zhou, W. Nie, Q. Zhang, W. Wang, Y. Zhang, C. He, ACS Appl. Mater. Interfaces 8 (2016) 33829–33841.
[38] Y.J. Cheng, A.Q. Zhang, J.J. Hu, F. He, X. Zeng, X.Z. Zhang, ACS Appl. Mater. Interfaces 9 (2017) 2093–2103.
[39] S.-M. Hsiao, B.-Y. Peng, Y.S. Tseng, H.-T. Liu, C.-H. Chen, H.-M. Lin, Microporous Mesoporous Mater. 250 (2017) 210–220.
[40] X. Li, C. Xie, H. Xia, Z. Wang, Langmuir 34 (2018) 9974–9981.
[41] S. Ren, J. Yang, L. Ma, X. Li, W. Wu, C. Liu, J. He, L. Miao, ACS Appl. Mater. Interfaces 10 (2018) 31947–31958.
[42] Q. Sun, Q. You, J. Wang, L. Liu, Y. Wang, Y. Song, Y. Cheng, S. Wang, F. Tan, N. Li, ACS Appl. Mater. Interfaces 10 (2018) 1963–1975.

[43] Z. Yang, W. Fan, J. Zou, W. Tang, L. Li, L. He, Z. Shen, Z. Wang, O. Jacobson, M. A. Aronova, P. Rong, J. Song, W. Wang, X. Chen, J. Am. Chem. Soc. 141 (2019) 14687–14698.
[44] C. Wang, L. Cheng, Z. Liu, Theranostics 3 (2013) 317–330.
[45] G. Tian, X. Zhang, Z. Gu, Y. Zhao, Adv. Mater. 27 (2015) 7692–7712.
[46] S.K. Tripathi, G. Kaur, R.K. Khurana, S. Kapoor, B. Singh, Crit. Rev. Ther. Drug Carrier Syst. 32 (2015) 461–502.
[47] O.S. Wolfbeis, Chem. Soc. Rev. 44 (2015) 4743–4768.
[48] M.-X. Zhao, B.-J. Zhu, Nanoscale Res. Lett. 11 (2016) 207.
[49] C. Matea, T. Mocan, F. Tabaran, T. Pop, O. Mosteanu, C. Puia, C. Iancu, L. Mocan, Int. J. Nanomedicine 12 (2017) 5421–5431.
[50] X. Liu, I. Que, X. Kong, Y. Zhang, L. Tu, Y. Chang, T.T. Wang, A. Chan, C.W.G. M. Löwik, H. Zhang, Nanoscale 7 (2015) 14914–14923.
[51] G. Chen, H. Qiu, P.N. Prasad, X. Chen, Chem. Rev. 114 (2014) 5161–5214.
[52] R. Lv, D. Wang, L. Xiao, G. Chen, J. Xia, P.N. Prasad, Sci. Rep. 7 (2017) 15753.
[53] G. Xu, G. Lin, S. Lin, N. Wu, Y. Deng, G. Feng, Q. Chen, J. Qu, D. Chen, S. Chen, H. Niu, S. Mei, K.-T. Yong, X. Wang, Sci. Rep. 6 (2016) 37677.
[54] C. Dong, Z. Liu, L. Zhang, W. Guo, X. Li, J. Liu, H. Wang, J. Chang, ACS Appl. Mater. Interfaces 7 (2015) 7566–7575.
[55] J. Song, Y. Zhang, Y. Dai, J. Hu, L. Zhu, X. Xu, Y. Yu, H. Li, B. Yao, H. Zhou, ACS Appl. Mater. Interfaces 11 (2019) 9884–9892.
[56] H. Liu, F. Ren, X. Zhou, C. Ma, T. Wang, H. Zhang, Q. Sun, Z. Li, Anal. Chem. 91 (2019) 15064–15072.
[57] E.H. Ang, J. Zeng, G.S. Subramanian, V. Chellappan, T. Sudhaharan, P. Padmanabhan, B. Gulyás, S. Tamil Selvan, ACS Appl. Nano Mater. 3 (2020) 3088–3096.
[58] M. Thakur, A. Mewada, S. Pandey, M. Bhori, K. Singh, M. Sharon, M. Sharon, Mater. Sci. Eng. C 67 (2016) 468–477.
[59] Y. Il Park, K.T. Lee, Y.D. Suh, T. Hyeon, Chem. Soc. Rev. 44 (2015) 1302–1317.
[60] X. Huang, W. Zhang, G. Guan, G. Song, R. Zou, J. Hu, Acc. Chem. Res. 50 (2017) 2529–2538.
[61] R. Liu, M. Lv, Q. Wang, H. Li, P. Guo, X.S. Zhao, J. Magn. Magn. Mater. 424 (2017) 155–160.
[62] Y. Yong, X. Cheng, T. Bao, M. Zu, L. Yan, W. Yin, C. Ge, D. Wang, Z. Gu, Y. Zhao, ACS Nano 9 (2015) 12451–12463.
[63] W. Du, Y. Yuan, L. Wang, Y. Cui, H. Wang, H. Xu, G. Liang, Bioconjug. Chem. 26 (2015) 2571–2578.
[64] W. Guo, Z. Qiu, C. Guo, D. Ding, T. Li, F. Wang, J. Sun, N. Zheng, S. Liu, ACS Appl. Mater. Interfaces 9 (2017) 9348–9358.
[65] Y. Wang, Y. Wang, G. Chen, Y. Li, W. Xu, S. Gong, ACS Appl. Mater. Interfaces 9 (2017) 30297–30305.
[66] R. Lv, P. Yang, F. He, S. Gai, C. Li, Y. Dai, G. Yang, J. Lin, ACS Nano 9 (2015) 1630–1647.
[67] H. Qiao, Z. Cui, S. Yang, D. Ji, Y. Wang, Y. Yang, X. Han, Q. Fan, A. Qin, T. Wang, X.P. He, W. Bu, T. Tang, ACS Nano 11 (2017) 7259–7273.
[68] R.G. Mendes, A. Bachmatiuk, B. Büchner, G. Cuniberti, M.H. Rümmeli, J. Mater. Chem. B 1 (2013) 401–428.
[69] Y. Zhang, M. Wu, M. Wu, J. Zhu, X. Zhang, ACS Omega 3 (2018) 9126–9145.
[70] D. Chen, C.A. Dougherty, K. Zhu, H. Hong, J. Control. Release 210 (2015) 230–245.
[71] W. Yu, X. Cao, G. Xu, Y. Song, G. Li, H. Zheng, N. Zhang, Surgery 160 (2016) 755–761.
[72] X. Wu, Q. Lin, G. Chen, J. Lu, Y. Zeng, X. Chen, J. Yan, PLoS One 10 (2015), e0135714.
[73] H. Zhao, Y. Chao, J. Liu, J. Huang, J. Pan, W. Guo, J. Wu, M. Sheng, K. Yang, J. Wang, Z. Liu, Theranostics 6 (2016) 1833–1843.
[74] Z. Liu, S. Tabakman, S. Sherlock, X. Li, Z. Chen, K. Jiang, S. Fan, H. Dai, Nano Res. 3 (2010) 222–233.
[75] J.T.-W. Wang, K.T. Al-Jamal, Nanomedicine 10 (2015) 2639–2642.
[76] H. Kafa, J.T.-W. Wang, N. Rubio, K. Venner, G. Anderson, E. Pach, B. Ballesteros, J.E. Preston, N.J. Abbott, K.T. Al-Jamal, Biomaterials 53 (2015) 437–452.
[77] Z. Li, A.L.B. de Barros, D.C.F. Soares, S.N. Moss, L. Alisaraie, Int. J. Pharm. 524 (2017) 41–54.
[78] A. Eatemadi, H. Daraee, H. Karimkhanloo, M. Kouhi, N. Zarghami, A. Akbarzadeh, M. Abasi, Y. Hanifehpour, S. Joo, Nanoscale Res. Lett. 9 (2014) 393.
[79] C. Tchounwou, S.S. Sinha, B.P. Viraka Nellore, A. Pramanik, R. Kanchanapally, S. Jones, S.R. Chavva, P.C. Ray, ACS Appl. Mater. Interfaces 7 (2015) 20649–20656.
[80] K.H. Son, J.H. Hong, J.W. Lee, Int. J. Nanomedicine 11 (2016) 5163–5185.
[81] Z. Chen, A. Zhang, X. Wang, J. Zhu, Y. Fan, H. Yu and Z. Yang, J. Nanomater., DOI:https://doi.org/10.1155/2017/3418932.
[82] Z. Sobhani, M.A. Behnam, F. Emami, A. Dehghanian, I. Jamhiri, Int. J. Nanomedicine 12 (2017) 4509–4517.
[83] X. Dong, Z. Sun, X. Wang, X. Leng, Nanomedicine 13 (2017) 2271–2280.
[84] N. Li, Q. Zhao, C. Shu, X. Ma, R. Li, H. Shen, W. Zhong, Int. J. Pharm. 478 (2015) 644–654.
[85] T.K. Ryu, S.W. Baek, R.H. Kang, S.W. Choi, Adv. Funct. Mater. 26 (2016) 6428–6436.
[86] P. Kalluru, R. Vankayala, C.S. Chiang, K.C. Hwang, Biomaterials 95 (2016) 1–10.
[87] X. Liu, M. Peng, G. Li, Y. Miao, H. Luo, G. Jing, Y. He, C. Zhang, F. Zhang, H. Fan, Nano Lett. 19 (2019) 4118–4125.
[88] Y.W. Chen, P.J. Chen, S.H. Hu, I.W. Chen, S.Y. Chen, Adv. Funct. Mater. 24 (2014) 451–459.
[89] D. Hu, J. Zhang, G. Gao, Z. Sheng, H. Cui, L. Cai, Theranostics 6 (2016) 1043–1052.
[90] R. Imani, W. Shao, S. Taherkhani, S.H. Emami, S. Prakash, S. Faghihi, Colloids Surf. B: Biointerfaces 147 (2016) 315–325.
[91] D.Y. Zhang, Y. Zheng, C.P. Tan, J.H. Sun, W. Zhang, L.N. Ji, Z.W. Mao, ACS Appl. Mater. Interfaces 9 (2017) 6761–6771.
[92] J. Ge, M. Lan, B. Zhou, W. Liu, L. Guo, H. Wang, Q. Jia, G. Niu, X. Huang, H. Zhou, X. Meng, P. Wang, C.-S. Lee, W. Zhang, X. Han, Nat. Commun. 5 (2014) 4596.
[93] X. Sui, C. Luo, C. Wang, F. Zhang, J. Zhang, S. Guo, Nanomedicine 12 (2016) 1997–2006.
[94] D. Iannazzo, A. Pistone, M. Salamò, S. Galvagno, R. Romeo, S.V. Giofré, C. Branca, G. Visalli, A. Di Pietro, Int. J. Pharm. 518 (2017) 185–192.
[95] S. De, K. Patra, D. Ghosh, K. Dutta, A. Dey, G. Sarkar, J. Maiti, A. Basu, D. Rana, D. Chattopadhyay, ACS Biomater Sci. Eng. 4 (2018) 514–531.
[96] R.K. Singh, K.D. Patel, C. Mahapatra, M.S. Kang, H.W. Kim, ACS Appl. Mater. Interfaces 8 (2016) 24433–24444.
[97] J. Ge, Q. Jia, W. Liu, M. Lan, B. Zhou, L. Guo, H. Zhou, H. Zhang, Y. Wang, Y. Gu, X. Meng, P. Wang, Adv. Healthc. Mater. 5 (2016) 665–675.
[98] Q. Jia, J. Ge, W. Liu, L. Guo, X. Zheng, S. Chen, M. Chen, S. Liu, L. Zhang, M. Wang, H. Zhang, P. Wang, Adv. Healthc. Mater. 6 (2017), 1601419.
[99] C. Scialabba, A. Sciortino, F. Messina, G. Buscarino, M. Cannas, G. Roscigno, G. Condorelli, G. Cavallaro, G. Giammona, N. Mauro, ACS Appl. Mater. Interfaces 11 (2019) 19854–19866.
[100] J. Conde, G. Doria and P. Baptista, J. Drug Deliv., 2012, **2012**, 1–12.
[101] A. Khan, R. Rashid, G. Murtaza, A. Zahra, Trop. J. Pharm. Res. 13 (2014) 1169.
[102] A.J. Clark, M.E. Davis, Proc. Natl. Acad. Sci. 112 (2015) 12486–12491.
[103] F. Y. Kong, J. W. Zhang, R. F. Li, Z. X. Wang, W. J. Wang and W. Wang, Molecules, DOI:https://doi.org/10.3390/molecules22091445.
[104] S. Kazuma, D. Sultan, Y. Zhao, L. Detering, M. You, H. Luehmann, D. Abdalla, Y. Liu, Curr. Pharm. Des. 21 (2015) 5267–5276.
[105] C. Yao, L. Zhang, J. Wang, Y. He, J. Xin, S. Wang, H. Xu, Z. Zhang, J. Nanomater. 2016 (2016) 1–29.
[106] H. Deng, Y. Zhong, M. Du, Q. Liu, Z. Fan, F. Dai, X. Zhang, Theranostics 4 (2014) 904–918.
[107] P. Di Pietro, G. Strano, L. Zuccarello, C. Satriano, Curr. Top. Med. Chem. 16 (2016) 3069–3102.
[108] M. Yamada, M. Foote, T.W. Prow, Wiley Interdiscip. Rev. Nanomed. Nanobiotechnol. 7 (2015) 428–445.
[109] L. Tian, L. Lu, Y. Qiao, S. Ravi, F. Salatan, M. Melancon, J. Funct. Biomater. 7 (2016) 19.
[110] R. Mendes, A. Fernandes, P. Baptista, Genes (Basel) 8 (2017) 94.
[111] P. Tiwari, K. Vig, V. Dennis, S. Singh, Nanomaterials 1 (2011) 31–63.
[112] R.M. Cabral, P.V. Baptista, Expert. Rev. Mol. Diagn. 14 (2014) 1041–1052.
[113] E.C. Dreaden, L.A. Austin, M.A. Mackey, M.A. El-Sayed, Ther. Deliv. 3 (2012) 457–478.
[114] W. Chen, C. Ayala-Orozco, N.C. Biswal, C. Perez-Torres, M. Bartels, R. Bardhan, G. Stinnet, X.-D. Liu, B. Ji, A. Deorukhkar, L.V. Brown, S. Guha, R.G. Pautler, S. Krishnan, N.J. Halas, A. Joshi, Nanomedicine 9 (2014) 1209–1222.
[115] X. Tan, J. Wang, X. Pang, L. Liu, Q. Sun, Q. You, F. Tan, N. Li, ACS Appl. Mater. Interfaces 8 (2016) 34991–35003.
[116] V. De Matteis, M. Cascione, C. C. Toma and S. Leporatti, Nanomaterials, DOI: https://doi.org/10.3390/nano8050319.
[117] A.C. Burduşel, O. Gherasim, A.M. Grumezescu, L. Mogoantă, A. Ficai, E. Andronescu, Nanomaterials 8 (2018) 1–25.
[118] H. Chugh, D. Sood, I. Chandra, V. Tomar, G. Dhawan, R. Chandra, Artif. Cells Nanomed. Biotechnol. 46 (2018) 1210–1220.
[119] J. Swanner, R. Singh, Methods Mol. Biol. **1790** (2018) 209–218.
[120] Q. Wu, J. Yu, M. Li, L. Tan, X. Ren, C. Fu, Z. Chen, F. Cao, J. Ren, L. Li, P. Liang, Y. Zhang, X. Meng, Biomaterials 179 (2018) 122–133.
[121] M. Naz, N. Nasiri, M. Ikram, M. Nafees, M.Z. Qureshi, S. Ali, A. Tricoli, Appl. Nanosci. 7 (2017) 793–802.
[122] S. Gurunathan, J. Raman, S. N. Abd Malek, P. A. John and S. Vikineswary, Int. J. Nanomedicine, DOI:https://doi.org/10.2147/IJN.S51881.
[123] Y. He, Z. Du, S. Ma, S. Cheng, S. Jiang, Y. Liu, D. Li, H. Huang, K. Zhang and X. Zheng, Nanoscale Res. Lett., DOI:https://doi.org/10.1186/s11671-016-1511-9.
[124] S. R. Satapathy, P. Mohapatra, R. Preet, D. Das, B. Sarkar, T. Choudhuri, M. D. Wyatt and C. N. Kundu, Nanomedicine, DOI:https://doi.org/10.2217/nnm.12.176.
[125] S. Gurunathan, J. K. Jeong, J. W. Han, X. F. Zhang, J. H. Park and J. H. Kim, Nanoscale Res. Lett., DOI:https://doi.org/10.1186/s11671-015-0747-0.
[126] R. Sankar, A. Karthik, A. Prabu, S. Karthik, K. S. Shivashangari and V. Ravikumar, Colloids Surf. B: Biointerfaces, DOI:https://doi.org/10.1016/j.colsurfb.2013.02.033.
[127] K. Jadhav, S. Deore, D. Dhamecha, R. Hr, S. Jagwani, S. Jalalpure, R. Bohara, ACS Biomater Sci. Eng. 4 (2018) 892–899.
[128] P. Liu, H. Yang, W. Chen, J. Zhao and D. Li, J. Nanopart. Res., DOI:https://doi.org/10.1007/s11051-019-4703-2.
[129] J.Y. Li, L. Qiu, X.F. Xu, C.Y. Pan, C.Y. Hong, W.J. Zhang, J. Mater. Chem. B 6 (2018) 1678–1687.
[130] L. Qiu, J.W. Li, C.Y. Hong, C.Y. Pan, ACS Appl. Mater. Interfaces 9 (2017) 40887–40897.
[131] K. Sztandera, M. Gorzkiewicz, B. Klajnert-Maculewicz, Mol. Pharm. 16 (2019) 1–23.
[132] P. Singh, S. Pandit, V. R. S. S. Mokkapati, A. Garg, V. Ravikumar and I. Mijakovic, Int. J. Mol. Sci., DOI:https://doi.org/10.3390/ijms19071979.
[133] S. Wang, Y. Tian, W. Tian, J. Sun, S. Zhao, Y. Liu, C. Wang, Y. Tang, X. Ma, Z. Teng, G. Lu, ACS Nano 10 (2016) 8578–8590.

[134] L. Nie, S. Wang, X. Wang, P. Rong, Y. Ma, G. Liu, P. Huang, G. Lu, X. Chen, Small 10 (2014) 1585–1593.
[135] I.C. Sun, J.H. Na, S.Y. Jeong, D.E. Kim, I.C. Kwon, K. Choi, C.H. Ahn, K. Kim, Pharm. Res. 31 (2014) 1418–1425.
[136] B. Zhou, L. Zheng, C. Peng, D. Li, J. Li, S. Wen, M. Shen, G. Zhang, X. Shi, ACS Appl. Mater. Interfaces 6 (2014) 17190–17199.
[137] Y. Zhang, S. Wen, L. Zhao, D. Li, C. Liu, W. Jiang, X. Gao, W. Gu, N. Ma, J. Zhao, X. Shi and Q. Zhao, Nanoscale, DOI:https://doi.org/10.1039/c5nr07955a.
[138] V. Mulens-Arias, A. Nicolás-Boluda, A. Gehanno, A. Balfourier, F. Carn, F. Gazeau, Nanoscale 11 (2019) 3186–3192.
[139] T.M. Cheng, H.L. Chu, Y.C. Lee, D.Y. Wang, C.C. Chang, K.L. Chung, H.C. Yen, C. W. Hsiao, X.Y. Pan, T.R. Kuo, C.C. Chen, Anal. Chem. 90 (2018) 3974–3980.
[140] S. Zhu, X. Wang, S. Li, L. Liu, L. Li, ACS Appl. Mater. Interfaces 12 (2020) 11063–11071.
[141] Y. Wang, J. Chen, J. Irudayaraj, ACS Nano 5 (2011) 9718–9725.
[142] Y. H. Chen, C. Y. Tsai, P. Y. Huang, M. Y. Chang, P. C. Cheng, C. H. Chou, D. H. Chen, C. R. Wang, A. L. Shiau and C. L. Wu, Mol. Pharm., DOI:https://doi.org/10.1021/mp060132k.
[143] H. Karimi-Maleh, A.F. Shojaei, F. Karimi, K. Tabatabaeia, S. Shakeri, J. Nanostruct. 8 (2018) 417–424.
[144] S. Mondal, G. Hoang, P. Manivasagan, M.S. Moorthy, T.T. Vy Phan, H.H. Kim, T. P. Nguyen, J. Oh, Ceram. Int. 45 (2019) 2977–2988.
[145] J. Zhu, G. Wang, C.S. Alves, H. Tomás, Z. Xiong, M. Shen, J. Rodrigues, X. Shi, Langmuir 34 (2018) 12428–12435.
[146] E.L.L. Yeo, J.U.J. Cheah, P.S.P. Thong, K.C. Soo, J.C.Y. Kah, ACS Appl. Nano Mater. 2 (2019) 6220–6229.
[147] W. Chen, J. Ouyang, H. Liu, M. Chen, K. Zeng, J. Sheng, Z. Liu, Y. Han, L. Wang, J. Li, L. Deng, Y.-N. Liu, S. Guo, Adv. Mater. 29 (2017), 1603864.
[148] B. Navyatha, S. Nara, Nanomedicine 14 (2019) 767–796.
[149] K. Bera, S. Maiti, M. Maity, C. Mandal, N.C. Maiti, ACS Omega 3 (2018) 4602–4619.
[150] E.T. Vickers, M. Garai, S. Bonabi Naghadeh, S. Lindley, J. Hibbs, Q.H. Xu, J. Z. Zhang, J. Phys. Chem. C 122 (2018) 13304–13313.
[151] J. Wang, D. Liang, Q. Jin, J. Feng, X. Tang, Bioconjug. Chem. 31 (2020) 182–193.
[152] Y. Li, P. Li, R. Zhu, C. Luo, H. Li, S. Hu, Z. Nie, Y. Huang, S. Yao, Anal. Chem. 88 (2016) 11184–11192.
[153] B. Chatterjee, A. Ghoshal, A. Chattopadhyay, S.S. Ghosh, ACS Biomater Sci. Eng. 4 (2018) 1005–1012.
[154] D. Dutta, S.K. Sailapu, A. Chattopadhyay, S.S. Ghosh, ACS Appl. Mater. Interfaces 10 (2018) 3210–3218.
[155] A. Ghoshal, U. Goswami, A.K. Sahoo, A. Chattopadhyay, S.S. Ghosh, ACS Biomater Sci. Eng. 1 (2015) 1256–1266.
[156] L.L. Ma, J.O. Tam, B.W. Willsey, D. Rigdon, R. Ramesh, K. Sokolov, K.P. Johnston, Langmuir 27 (2011) 7681–7690.
[157] A.K. Sahoo, S. Banerjee, S.S. Ghosh, A. Chattopadhyay, ACS Appl. Mater. Interfaces 6 (2014) 712–724.
[158] T.T. Jia, G. Yang, S.J. Mo, Z.Y. Wang, B.J. Li, W. Ma, Y.X. Guo, X. Chen, X. Zhao, J.Q. Liu, S.Q. Zang, ACS Nano 13 (2019) 8320–8328.
[159] M. Wu, Z. Li, J. Yao, Z. Shao, X. Chen, ACS Biomater Sci. Eng. 5 (2019) 4799–4807.
[160] N. Verma, N. Kumar, ACS Biomater Sci. Eng. 5 (2019) 1170–1188.
[161] M. Zhou, M. Tian, C. Li, Bioconjug. Chem. 27 (2016) 1188–1199.
[162] U. Goswami, A. Dutta, A. Raza, R. Kandimalla, S. Kalita, S.S. Ghosh, A. Chattopadhyay, ACS Appl. Mater. Interfaces 10 (2018) 3282–3294.
[163] D. Chen, C. Zhao, J. Ye, Q. Li, X. Liu, M. Su, H. Jiang, C. Amatore, M. Selke, X. Wang, ACS Appl. Mater. Interfaces 7 (2015) 18163–18169.
[164] Z. Xie, S. Chen, Y. Duo, Y. Zhu, T. Fan, Q. Zou, M. Qu, Z. Lin, J. Zhao, Y. Li, L. Liu, S. Bao, H. Chen, D. Fan and H. Zhang, ACS Appl. Mater. Interfaces, DOI:https://doi.org/10.1021/acsami.9b04628.
[165] L. Dong, P. Zhang, X. Liu, R. Deng, K. Du, J. Feng, H. Zhang, ACS Appl. Mater. Interfaces 11 (2019) 7774–7781.
[166] Z. Skeete, H. Cheng, E. Crew, L. Lin, W. Zhao, P. Joseph, S. Shan, H. Cronk, J. Luo, Y. Li, Q. Zhang, C.J. Zhong, ACS Appl. Mater. Interfaces 6 (2014) 21752–21768.
[167] Y. Han, S. Gao, S. Gao, Y. Zhang, Q. Ni, Z. Li, X.J. Liang, J. Zhang, Bioconjug. Chem. 31 (2020) 1247–1258.
[168] X. Wang, X. Wang, Z. Guo, Acc. Chem. Res. 48 (2015) 2622–2631.
[169] B. Ghaemi, E. Shaabani, R. Najafi-Taher, S. Jafari Nodooshan, A. Sadeghpour, S. Kharrazi, A. Amani, ACS Appl. Mater. Interfaces 10 (2018) 24370–24381.
[170] S.K. Mishra, S. Kannan, ACS Biomater Sci. Eng. 3 (2017) 3607–3619.
[171] S.K. Mishra, S. Kannan, Langmuir 32 (2016) 13687–13696.
[172] A.K. Sahoo, U. Goswami, D. Dutta, S. Banerjee, A. Chattopadhyay, S.S. Ghosh, ACS Biomater Sci. Eng. 2 (2016) 1395–1402.
[173] L. Chen, H. Li, H. He, H. Wu, Y. Jin, Anal. Chem. 87 (2015) 6868–6874.
[174] Z. Zhang, C. Liu, J. Bai, C. Wu, Y. Xiao, Y. Li, J. Zheng, R. Yang, W. Tan, ACS Appl. Mater. Interfaces 7 (2015) 6211–6219.
[175] D. Dutta, A. Chattopadhyay, S.S. Ghosh, ACS Biomater Sci. Eng. 2 (2016) 2090–2098.
[176] B. Zhou, Z. Xiong, P. Wang, C. Peng, M. Shen, S. Mignani, J.P. Majoral, X. Shi, Drug Deliv. 25 (2018) 178–186.
[177] B. Zhou, Z. Xiong, J. Zhu, M. Shen, G. Tang, C. Peng and X. Shi, Nanomedicine, DOI:https://doi.org/10.2217/nnm-2016-0093.
[178] B. Zhou, J. Yang, C. Peng, J. Zhu, Y. Tang, X. Zhu, M. Shen, G. Zhang and X. Shi, Colloids Surf. B: Biointerfaces, DOI:https://doi.org/10.1016/j.colsurfb.2016.01.019.
[179] J. Wang, D. Wheeler, J.Z. Zhang, S. Achilefu, K.A. Kang, Adv. Exp. Med. Biol. 765 (2013) 323–328.
[180] J.D. Mangadlao, X. Wang, C. McCleese, M. Escamilla, G. Ramamurthy, Z. Wang, M. Govande, J.P. Basilion, C. Burda, ACS Nano 12 (2018) 3714–3725.
[181] Q. Dong, H. Yang, C. Wan, D. Zheng, Z. Zhou, S. Xie, L. Xu, J. Du and F. Li, Nanoscale Res. Lett., DOI:https://doi.org/10.1186/s11671-019-3053-4.
[182] L. Zhao, Y. Li, J. Zhu, N. Sun, N. Song, Y. Xing, H. Huang, J. Zhao, J. Nanobiotechnol. 17 (2019) 1–13.
[183] F. Emami, A. Banstola, A. Vatanara, S. Lee, J.O. Kim, J.H. Jeong, S. Yook, Mol. Pharm. 16 (2019) 1184–1199.
[184] B. Pang, Y. Zhao, H. Luehmann, X. Yang, L. Detering, M. You, C. Zhang, L. Zhang, Z.Y. Li, Q. Ren, Y. Liu, Y. Xia, ACS Nano 10 (2016) 3121–3131.
[185] N.R. Patel, A. Piroyan, A.H. Nack, C.A. Galati, M. McHugh, S. Orosz, A.W. Keeler, S. O'Neal, W.C. Zamboni, B. Davis, T.P. Coleman, Mol. Pharm. 13 (2016) 1996–2009.
[186] Wahajuddin, S. Arora, Int. J. Nanomedicine 7 (2012) 3445–3471.
[187] S. Fazal, B. Paul-Prasanth, S.V. Nair, D. Menon, ACS Appl. Mater. Interfaces 9 (2017) 28260–28272.
[188] G. Kandasamy, D. Maity, Int. J. Pharm. 496 (2015) 191–218.
[189] R. Hachani, M. Lowdell, M. Birchall, A. Hervault, D. Mertz, S. Begin-Colin, N.T. K. Thanh, Nanoscale 8 (2016) 3278–3287.
[190] G. Kandasamy, S. Surendran, A. Chakrabarty, S.N. Kale, D. Maity, RSC Adv. 6 (2016) 99948–99959.
[191] Z.R. Stephen, C.J. Dayringer, J.J. Lim, R.A. Revia, M.V. Halbert, M. Jeon, A. Bakthavatsalam, R.G. Ellenbogen, M. Zhang, ACS Appl. Mater. Interfaces 8 (2016) 6320–6328.
[192] D. Maity, P. Chandrasekharan, C.-T. Yang, K.-H. Chuang, B. Shuter, J.-M. Xue, J. Ding, S.-S. Feng, Nanomedicine 5 (2010) 1571–1584.
[193] D. Maity, P. Chandrasekharan, P. Pradhan, K.-H. Chuang, J.-M. Xue, S.-S. Feng, J. Ding, J. Mater. Chem. 21 (2011) 14717.
[194] R. Grillo, J. Gallo, D.G. Stroppa, E. Carbó-Argibay, R. Lima, L.F. Fraceto, M. Bañobre-López, ACS Appl. Mater. Interfaces 8 (2016) 25777–25787.
[195] J. Mosafer, K. Abnous, M. Tafaghodi, H. Jafarzadeh, M. Ramezani, Colloids Surf. A Physicochem. Eng. Asp. 514 (2017) 146–154.
[196] J. Mosafer, M. Teymouri, Artif. Cells Nanomed. Biotechnol. 46 (2018) 1146–1155.
[197] G. Kandasamy, A. Sudame, D. Maity, S. Soni, K. Sushmita, N.S. Veerapu, S. Bose, C.V. Tomy, J. Mol. Liq. 293 (2019), 111549.
[198] A. Sudame, G. Kandasamy, D. Singh, C.V. Tomy, D. Maity, Colloids Surf. A Physicochem. Eng. Asp. 606 (2020), 125355.
[199] H. Ma, Y. Liu, M. Shi, X. Shao, W. Zhong, W. Liao, M.M.Q. Xing, Biomacromolecules 16 (2015) 4022–4031.
[200] E.B. Ehlerding, P. Grodzinski, W. Cai, C.H. Liu, ACS Nano 12 (2018) 2106–2121.
[201] L. Zhu, Z. Zhou, H. Mao, L. Yang, Nanomedicine 12 (2017) 73–87.
[202] F. Lux, L. Sancey, A. Bianchi, Y. Crémillieux, S. Roux, O. Tillement, Nanomedicine 10 (2015) 1801–1815.
[203] J.P. Finn, K.-L. Nguyen, F. Han, Z. Zhou, I. Salusky, I. Ayad, P. Hu, Clin. Radiol. 71 (2016) 796–806.
[204] H.E. Daldrup-Link, Radiology 284 (2017) 616–629.
[205] G.B. Toth, C.G. Varallyay, A. Horvath, M.R. Bashir, P.L. Choyke, H.E. Daldrup-Link, E. Dosa, J.P. Finn, S. Gahramanov, M. Harisinghani, I. Macdougall, A. Neuwelt, S.S. Vasanawala, P. Ambady, R. Barajas, J.S. Cetas, J. Ciporen, T. J. DeLoughery, N.D. Doolittle, R. Fu, J. Grinstead, A.R. Guimaraes, B.E. Hamilton, X. Li, H.L. McConnell, L.L. Muldoon, G. Nesbit, J.P. Netto, D. Petterson, W. D. Rooney, D. Schwartz, L. Szidonya, E.A. Neuwelt, Kidney Int. 92 (2017) 47–66.
[206] Y.-W. Jun, Y.-M. Huh, J.-S. Choi, J.-H. Lee, H.-T. Song, S. Kim, S. Yoon, K.-S. Kim, J.-S. Shin, J.-S. Suh, J. Cheon, J. Am. Chem. Soc. 127 (2005) 5732–5733.
[207] D. Maity, G. Zoppellaro, V. Sedenkova, J. Tucek, K. Safarova, K. Polakova, K. Tomankova, C. Diwoky, R. Stollberger, L. Machala, R. Zboril, Chem. Commun. 48 (2012) 11398.
[208] B. Karagoz, J. Yeow, L. Esser, S.M. Prakash, R.P. Kuchel, T.P. Davis, C. Boyer, Langmuir 30 (2014) 10493–10502.
[209] Z.W. Tay, P. Chandrasekharan, A. Chiu-Lam, D.W. Hensley, R. Dhavalikar, X. Y. Zhou, E.Y. Yu, P.W. Goodwill, B. Zheng, C. Rinaldi, S.M. Conolly, ACS Nano 12 (2018) 3699–3713.
[210] G. Kandasamy, A. Sudame, P. Bhati, A. Chakrabarty, S.N. Kale, D. Maity, J. Colloid Interface Sci. 514 (2018) 534–543.
[211] G. Kandasamy, A. Sudame, P. Bhati, A. Chakrabarty, D. Maity, J. Mol. Liq. 256 (2018) 224–237.
[212] G. Kandasamy, A. Sudame, T. Luthra, K. Saini, D. Maity, ACS Omega 3 (2018) 3991–4005.
[213] G. Kandasamy, S. Soni, K. Sushmita, N.S. Veerapu, S. Bose, D. Maity, J. Mol. Liq. 274 (2019) 653–663.
[214] G. Kandasamy, S. Khan, J. Giri, S. Bose, N.S. Veerapu, D. Maity, J. Mol. Liq. 275 (2019) 699–712.
[215] C. Prashant, M. Dipak, C.-T. Yang, K.-H. Chuang, D. Jun, S.-S. Feng, Biomaterials 31 (2010) 5588–5597.
[216] P. Chandrasekharan, D. Maity, C.X. Yong, K.H. Chuang, J. Ding, S.S. Feng, Biomaterials 32 (2011) 5663–5672.
[217] A. Salunkhe, V. Khot, S.I. Patil, S.A.M. Tofail, J. Bauer, N.D. Thorat, ACS Appl. Bio Mater. 3 (2020) 2305–2313.
[218] J.S. Basuki, H.T.T. Duong, A. Macmillan, R.B. Erlich, L. Esser, M.C. Akerfeldt, R. M. Whan, M. Kavallaris, C. Boyer, T.P. Davis, ACS Nano 7 (2013) 10175–10189.
[219] C. Kaewsaneha, P. Tangboriboonrat, D. Polpanich, A. Elaissari, ACS Appl. Mater. Interfaces 7 (2015) 23373–23386.
[220] L. Yan, L. Luo, A. Amirshaghaghi, J. Miller, C. Meng, T. You, T.M. Busch, A. Tsourkas, Z. Cheng, Bioconjug. Chem. 30 (2019) 2974–2981.

[221] J. Qin, Q. Liu, J. Zhang, J. Chen, S. Chen, Y. Zhao, J. Du, ACS Appl. Mater. Interfaces 7 (2015) 14043–14052.
[222] M. Rasekh, Z. Ahmad, R. Cross, J. Hernández-Gil, J.D.E.T. Wilton-Ely, P. W. Miller, Mol. Pharm. 14 (2017) 2010–2023.
[223] D. Luong, S. Sau, P. Kesharwani, A.K. Iyer, Biomacromolecules 18 (2017) 1197–1209.
[224] T.D. Schladt, K. Schneider, H. Schild, W. Tremel, Dalton Trans. 40 (2011) 6315–6343.
[225] F. Chen, P.A. Ellison, C.M. Lewis, H. Hong, Y. Zhang, S. Shi, R. Hernandez, M. E. Meyerand, T.E. Barnhart, W. Cai, Angew. Chem. Int. Ed. 52 (2013) 13319–13323.
[226] G. Yang, H. Gong, T. Liu, X. Sun, L. Cheng, Z. Liu, Biomaterials 60 (2015) 62–71.
[227] H. Mok, M. Zhang, Expert Opin. Drug Deliv. 10 (2013) 73–87.
[228] A. P., M.M. Sophie Laurent, Amir Ata Saei, Shahed Behzadi, S. Laurent, A.A. Saei, S. Behzadi, A. Panahifar, M. Mahmoudi, Expert Opin. Drug Deliv. 11 (2014) 1449–1470.
[229] H. Zhou, W. Qian, F.M. Uckun, L. Wang, Y.A. Wang, H. Chen, D. Kooby, Q. Yu, M. Lipowska, C.A. Staley, H. Mao, L. Yang, ACS Nano 9 (2015) 7976–7991.
[230] G.Y. Lee, W.P. Qian, L. Wang, Y.A. Wang, C.A. Staley, M. Satpathy, S. Nie, H. Mao, L. Yang, ACS Nano 7 (2013) 2078–2089.
[231] J. Estelrich, E. Escribano, J. Queralt, M. Busquets, Int. J. Mol. Sci. 16 (2015) 8070–8101.
[232] K. Zhu, Z. Deng, G. Liu, J. Hu, S. Liu, Macromolecules 50 (2017) 1113–1125.
[233] K. Kaaki, K. Hervé-Aubert, M. Chiper, A. Shkilnyy, M. Soucé, R. Benoit, A. Paillard, P. Dubois, M.L. Saboungi, I. Chourpa, Langmuir 28 (2012) 1496–1505.
[234] F.M. Kievit, Z.R. Stephen, O. Veiseh, H. Arami, T. Wang, V.P. Lai, J.O. Park, R. G. Ellenbogen, M.L. Disis, M. Zhang, ACS Nano 6 (2012) 2591–2601.
[235] K. Hayashi, M. Nakamura, W. Sakamoto, T. Yogo, H. Miki, S. Ozaki, M. Abe, T. Matsumoto, K. Ishimura, Theranostics 3 (2013) 366–376.
[236] A. Ereath Beeran, F.B. Fernandez, P.R.H. Varma, ACS Biomater Sci. Eng. 5 (2019) 106–113.
[237] M.H. El-Dakdouki, D.C. Zhu, K. El-Boubbou, M. Kamat, J. Chen, W. Li, X. Huang, Biomacromolecules 13 (2012) 1144–1151.
[238] M.H. El-Dakdouki, J. Xia, D.C. Zhu, H. Kavunja, J. Grieshaber, S. O'Reilly, J. J. McCormick, X. Huang, ACS Appl. Mater. Interfaces 6 (2014) 697–705.
[239] D. Šmejkalová, K. Nešporová, G. Huerta-Angeles, J. Syrovátka, D. Jirák, A. Gálisová, V. Velebný, Biomacromolecules 15 (2014) 4012–4020.
[240] S. Wu, X. Liu, J. He, H. Wang, Y. Luo, W. Gong, Y. Li, Y. Huang, L. Zhong and Y. Zhao, Nanoscale Res. Lett., DOI:https://doi.org/10.1186/s11671-019-3049-0.
[241] G. Huang, H. Chen, Y. Dong, X. Luo, H. Yu, Z. Moore, E.A. Bey, D.A. Boothman, J. Gao, Theranostics 3 (2013) 116–126.
[242] W.H. Chiang, V.T. Ho, H.H. Chen, W.C. Huang, Y.F. Huang, S.C. Lin, C.S. Chern, H.C. Chiu, Langmuir 29 (2013) 6434–6443.
[243] C.M. Lee, S.J. Cheong, E.M. Kim, S.T. Lim, Y.Y. Jeong, M.H. Sohn, H.J. Jeong, J. Nucl. Med. 54 (2013) 1974–1980.
[244] A. Carrouée, E. Allard-Vannier, S. Meîme, F. Szeremeta, J.C. Beloeil, I. Chourpa, Anal. Chem. 87 (2015) 11233–11241.
[245] L. Chen, X. Zhou, W. Nie, W. Feng, Q. Zhang, W. Wang, Y. Zhang, Z. Chen, P. Huang, C. He, ACS Appl. Mater. Interfaces 9 (2017) 17786–17798.
[246] A. Manigandan, V. Handi, N.S. Sundaramoorthy, R. Dhandapani, J. Radhakrishnan, S. Sethuraman, A. Subramanian, Bioconjug. Chem. 29 (2018) 275–286.
[247] Y. Wang, L. Jiang, Y. Zhang, Y. Lu, J. Li, H. Wang, D. Yao, D. Wang, ACS Appl. Mater. Interfaces 12 (2020) 33564–33574.
[248] A. Tiwari, A. Singh, A. Debnath, A. Kaul, N. Garg, R. Mathur, A. Singh, J. K. Randhawa, ACS Appl. Nano Mater. 2 (2019) 3060–3072.
[249] V.M. Vijayan, A.E. Beeran, S.J. Shenoy, J. Muthu, V. Thomas, ACS Appl. Bio Mater. 2 (2019) 757–768.
[250] B. Das, A. Girigoswami, A. Dutta, P. Pal, J. Dutta, P. Dadhich, P.K. Srivas, S. Dhara, ACS Biomater Sci. Eng. 5 (2019) 3549–3560.
[251] A. Pan, M.G. Jakaria, S.A. Meenach, G.D. Bothun, ACS Appl. Bio Mater. 3 (2020) 273–281.
[252] A. Tiwari, N.C. Verma, S. Turkkan, A. Debnath, A. Singh, G. Draeger, C.K. Nandi, J.K. Randhawa, ACS Appl. Nano Mater. 3 (2020) 896–904.
[253] Z. Fan, D. Senapati, A.K. Singh, P.C. Ray, Mol. Pharm. 10 (2013) 857–866.
[254] M. Zhang, Y. Cao, L. Wang, Y. Ma, X. Tu, Z. Zhang, ACS Appl. Mater. Interfaces 7 (2015) 4650–4658.
[255] L. Sancey, S. Kotb, C. Truillet, F. Appaix, A. Marais, E. Thomas, B. Van Der Sanden, J.P. Klein, B. Laurent, M. Cottier, R. Antoine, P. Dugourd, G. Panczer, F. Lux, P. Perriat, V. Motto-Ros, O. Tillement, ACS Nano 9 (2015) 2477–2488.
[256] N.D. Thorat, R.A. Bohara, M.R. Noor, D. Dhamecha, T. Soulimane, S.A.M. Tofail, ACS Biomater Sci. Eng. 3 (2017) 1332–1340.
[257] J. Kim, H.R. Cho, H. Jeon, D. Kim, C. Song, N. Lee, S.H. Choi, T. Hyeon, J. Am. Chem. Soc. 139 (2017) 10992–10995.
[258] D. Patra, S. Mukherjee, I. Chakraborty, T.K. Dash, S. Senapati, R. Bhattacharyya, R. Shunmugam, ACS Biomater Sci. Eng. 4 (2018) 1738–1749.
[259] Z. Chu, Z. Wang, L. Chen, X. Wang, C. Huang, M. Cui, D.P. Yang, N. Jia, ACS Appl. Nano Mater. 1 (2018) 2332–2340.
[260] J. Wang, Y. Guo, J. Hu, W. Li, Y. Kang, Y. Cao, H. Liu, Langmuir 34 (2018) 9516–9524.
[261] Y. Sun, C. Yan, J. Xie, D. Yan, K. Hu, S. Huang, J. Liu, Y. Zhang, N. Gu, F. Xiong, ACS Appl. Mater. Interfaces 11 (2019) 29536–29548.